

# HIGH EFFICIENCY METHANOL CARBONYLATION PROCESS UTILIZING A GAS STRIPPED REACTOR AND IONIC LIQUID CATALYST SYSTEM

Gerald C. Tustin

Eastman Chemical Company  
P.O. Box 1972  
Kingsport, TN 37662

## Introduction

Acetic acid (HOAc) is a commodity chemical with an annual worldwide demand in excess of 6.9 million metric tons.<sup>1</sup> Most of the acetic acid produced today is prepared by the carbonylation of methanol. Many technologies have been examined, and those examined up to 1993 are summarized in a review article.<sup>2</sup> The greatest advance in methanol carbonylation technology was the discovery of a homogeneous iodide-promoted rhodium catalyst system introduced by Monsanto. This technology was vastly superior to all previous technologies and was characterized by modest pressures (450-500 psig) and temperatures (175-190°C), high methanol conversions (99-100%), high acetyl selectivities from methanol (99-100%), and excellent rates (approximately 6 moles acetic acid/L-hr).

Although the original rhodium-catalyzed carbonylation process was a technical breakthrough, it was not perfect. The process requires approximately 14-15 wt. % water to maintain catalyst activity. Removal of this water is expensive. The catalyst also catalyzes the water gas shift reaction under methanol carbonylation conditions, and a loss of carbon monoxide efficiency results. Catalyst recycle is also a concern. The product is flashed at about 65 psig and 166°C after it leaves the reactor. The heel from the flash process contains the rhodium catalyst which is recycled to the reactor. If the depth of flash is too great, if there is not enough water present, or if the CO pressure is too low, the catalyst precipitates and fouls the evaporator. The flash process is a major bottleneck in the methanol carbonylation process.

Two technological advances have improved the methanol carbonylation process. One of these is the addition of lithium iodide to the Rh catalyst system.<sup>3</sup> The presence of the added salt resulted in a substantial increase in reaction rate. The Rh-Li system also allowed for the water level to be reduced to 4-5 wt. % which increased the CO efficiency from about 91 % to 97 % and lowered water separation costs. The depth of flash was also increased. Another major advance was the replacement of the rhodium catalyst with an iridium-ruthenium catalyst.<sup>4</sup> The process improvements resulting from the use of the Ir-Ru catalyst are comparable to those exhibited by the Rh-Li system.

Although significant improvements over the original Rh-catalyzed carbonylation process have occurred, several major opportunities for further improvement exist. These include elimination of the flash evaporator and further reduction in the water and methyl acetate (MeOAc) in the product exiting the reactor. Although several attempts have been made to operate the carbonylation process in the vapor phase with heterogeneous catalysts, none have been commercialized.<sup>2</sup>

The study presented herein describes another approach to catalyst immobilization: the use of a gas stripped reactor containing active catalysts dissolved in ionic liquids. Ionic liquids are appealing for this application because they have essentially no vapor pressure and hence stay in the reactor while products leave as vapor, they are thermally stable and reasonably inert under the reaction conditions, and they provide effective heat removal. Ionic liquids containing iodide ion solubilize the metal catalyst, stabilize the metal in its

active state, and prevent the metal from volatilizing from the reaction mixture.

## Experimental

**Materials.** Rhodium trichloride hydrate was provided by Johnson Matthey. Iridium trichloride hydrate was provided by Strem Chemicals. Palladium acetate was obtained from Aldrich. Butyltridodecylphosphonium iodide (BTDPPI) was obtained from Cytec. 1-butyl-3-methylimidazolium iodide (BMIMI) was synthesized by the following procedure. 1-butylimidazole (400 g, 3.22 moles) was dissolved in tetrahydrofuran (400 mL) in a 3-liter flask equipped with a magnetic stir bar, reflux condenser and a pressure-equilibrated dropping funnel with a nitrogen inlet. Methyl iodide (570 g, 4.0 moles) was added from the addition funnel with stirring under nitrogen over seven hours at ambient temperature. The mixture was stirred for 2 hours at room temperature then refluxed overnight. The solvent and excess methyl iodide were then removed by distillation on a steam bath to provide BMIMI as a red-brown oil (870.7g). Methyltributylphosphonium iodide (MTBPI) was synthesized in an analogous fashion from tributylphosphine and methyl iodide. Methanol (MeOH) and methyl iodide (MeI) were reagent grade and were used without further purification.

**Carbonylation reactions.** The carbonylation procedure has been described in detail in the patent literature.<sup>5</sup> A brief but sufficient description will be provided here. The basic reaction system consisted of Brooks 5850 Series E mass flow controllers for gas delivery and an Alltech 301 HPLC pump for liquid feed delivery. The gas and liquid streams were fed to an electrically heated Hastelloy C vaporizer. The vaporized reactants were fed to an electrically heated Hastelloy C reactor containing the ionic liquid and catalyst, and the vapor product directed to a Hastelloy C condenser and product receiver. Pressure was maintained using a Tescom Model 44-2300 backpressure regulator. Heating and gas flow feeds were controlled by a Camile® 3300 Process Monitoring and Control System. Most of the reactions were performed in an unstirred reactor consisting of a 1.60 cm I.D. X 15.9 cm long Hastelloy C reaction tube fitted with a 5 micron Hastelloy C filter at the base which acted as a gas dispersion device and support for the ionic liquid catalyst system. Typical ionic liquid charge to the unstirred reactor was 10 mL which contained 0.32 mmole Rh. Some reactions were performed in a stirred 300 mL Hastelloy C autoclave with subsurface gas feed using the same feed and condensation systems used with the unstirred reactor. A typical ionic liquid charge to the stirred autoclave was 100 mL containing 3.2 mmoles Rh. Typical reaction pressures ranged between 200 and 250 psig, and typical reactor temperatures ranged between 190 and 250°C. Feed rates varied widely and are provided in the Results and Discussion section. Condensed methanol carbonylation products from the receiver were weighed and analyzed by gas chromatography using a 30 m X 0.25 mm DB-FFAP capillary column (0.25 micron thickness) programmed at 40°C for 5 minutes, 25°C/minute to 240°C and holding at 240°C for 1 minute using a thermal conductivity detector held at 250°C (injector temperature = 250°C).

## Results and Discussion

Initial continuous methanol carbonylation experiments were performed in the unstirred reactor with a 10 mL charge of BMIMI containing 0.32 mmole Rh catalyst at 190°C and 200 psig with a 2.8 CO/1.0 MeOH/0.14 MeI molar ratio feed. The results are summarized in **Figure 1** which illustrates the acetic acid and methyl acetate space time yields and methanol conversions at three different space velocities (153, 302 and 455 hr<sup>-1</sup>) over a period in excess of 200 hours. Essentially no decline in catalyst activity was observed over the duration of the experiment. At high space velocity, HOAc

space time yields exceeding 20 moles/L-hr were observed with about 90 % MeOH conversion. At the lowest space velocity the HOAc space time yield decreased, the HOAc/MeOAc ratio increased, and the methanol conversion approached 100 %. Acetaldehyde or propionic acid were not detected, and the condensed product contained only ppb levels of Rh. NMR analysis of the recovered ionic liquid revealed that about half of the butyl groups had been replaced by methyl groups but was otherwise unchanged.

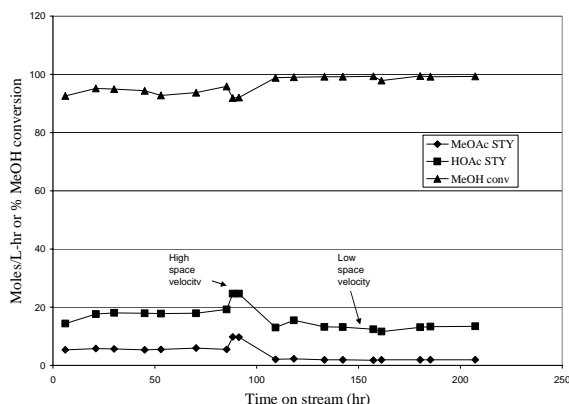


**Figure 1.** Space time yields and methanol conversions with the Rh/BMIMI catalyst system.

Although the initial results with the Rh/BMIMI catalyst system were very encouraging, the process used a large excess of CO. A CO conversion of approximately 70 % per pass is required for the process to be commercially attractive. Thus efforts focused on finding conditions that would allow for high CO conversion while retaining high methanol conversion and providing a product containing the lowest amounts of water and methyl acetate.

Two other metals were found to be active in the ionic liquid system: Pd and Ir. With the same temperature, pressure and reactant stream at a space velocity (SV) = 153 hr<sup>-1</sup>, when Rh was replaced with Pd (0.325 mmole) in the 10 mL BMIMI ionic liquid, HOAc and MeOAc were produced at 2.4 and 3.6 moles/L-hr respectively at 59 % methanol conversion. This observation was interesting since Pd is normally a very poor methanol carbonylation catalyst, but the ability of high concentrations of iodide to promote methanol carbonylation with Pd has been reported in the literature.<sup>6</sup> Iridium is poisoned by excess iodide ion, and a soft Lewis base is needed to control the iodide level.<sup>4</sup> Therefore the Iridium system was prepared with Ir (0.30 mmole), Ru, Li in a 1/5/1 molar ratio respectively in 10 mL of a mixture prepared from a 2/1 molar ratio ZnI<sub>2</sub>/BTDPI. At SV = 302 hr<sup>-1</sup>, the iridium system produced HOAc and MeOAc at 4 and 5 moles/L-hr respectively at 92 % methanol conversion. Although Pd and Ir metals were active catalysts, Rh had the highest activity. Further development work was therefore directed towards optimizing the Rh system.

Although rhodium was examined in several different ionic liquids, three will be discussed here: BMIMI, BTDPI and MTBPI. For each salt, conditions were adjusted to optimize conversions. As conversions increase the vapor contains less CO, MeOH, MeOAc and water and more HOAc, and conditions need to be adjusted to keep the product in the vapor phase. This can be accomplished by lowering the pressure, by increasing the temperature or both. Since the phosphonium salts are more thermally stable than the imidazolium salt they were evaluated at higher temperatures and pressures whereas BMIMI was evaluated at lower temperatures and

pressures. Definite differences were observed among the salts. For example, at 190°C BMIMI provided the highest carbonylation rates, but at 210°C BTDPI provided the highest CO conversion (77 %), and at 220°C MTBPI provided the highest HOAc/MeOAc ratio (38). To understand the differences among the three salts, a study of mass transfer effects was performed in the stirred autoclave using the 2.8 CO/1.0 MeOH/0.14 MeI feed at SV = 153 hr<sup>-1</sup>. **Figure 2** summarizes the results.

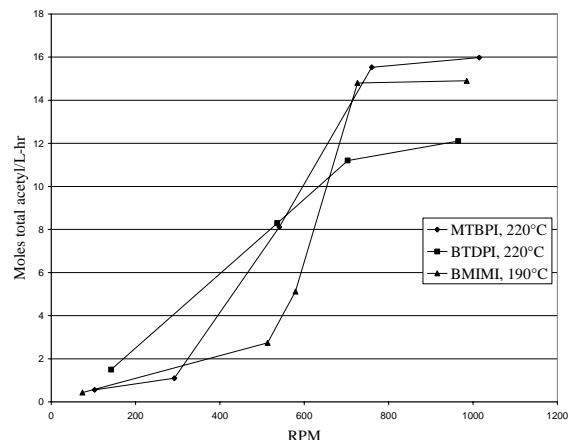


**Figure 2.** Total acetyl production rate at various stirring rates.

At low stirring rate the catalyst is not in its active state, there are no water gas shift products in the vent gas and abundant methyl ether is produced. As the stirring rate increases the catalyst becomes active, the vent gas contains water gas shift products, and negligible methyl ether is produced. The ultimate rates achieved appear to correlate inversely with the ionic liquid melt viscosity at reaction temperature (25 cp for MTBPI, 37 cp for BMIMI and 51 cp for BTDPI).

Eventually conditions were optimized utilizing MTBPI as the preferred ionic liquid to provide commercially acceptable performance. When 1.28 CO/1.0 MeOH/0.1 MeI molar ratio were fed at SV = 110 hr<sup>-1</sup> to a 0.057 molar Rh in MTBPI at 230°C and 225 psig, acetic acid was produced at a rate of 17 moles/L-hr at 76 % CO conversion and 100% MeOH conversion. The HOAc/MeOH ratio was 18 and the product contained only 1.1 wt. % water.

## Conclusions

Iodide-containing ionic liquids provide an excellent medium for vapor phase methanol carbonylation and eliminate the need for a separate flash evaporator. The high rate of reaction coupled with the very high purity of the product result in reduced reactor costs, reduced liquid recycle and separation costs.

**Acknowledgement.** The author acknowledges Eastman Chemical Company for supporting this work and Regina Moncier for technical assistance.

## References

- (1) Anon., *Chemical Week* **2004**, June 30/July 7, 40.
- (2) Howard, M.J., Jones, M.D., Roberts, M.S., Taylor, S.A., *Catalysis Today* **1993**, *18*, 325.
- (3) Smith, B.L., Torrence, G.P., Murphy, M.A., Aguilo, A., *Journal of Molecular Catalysis* **1987**, *39*, 115.
- (4) Sunley, G.J., Watson, D.J., *Catalysis Today* **2000**, *58*, 293.
- (5) Tustin, G.C., Moncier, R.M., International Publication Number WO 03/093211, **2003**.
- (6) Yang, J., Haynes, A., Maitlis, P.M., *Chem. Commun.* **1999**, 179.

# EFFECT OF PROCESS PARAMETERS ON LIGHT OLEFINS PRODUCTION FROM METHANOL AND SYNGAS OVER SAPO CATALYSTS

Luckner Jean<sup>a</sup>, Xiwen Huang<sup>a</sup> and James A. Guin<sup>a</sup>  
Gregory C. Turpin<sup>b</sup> and Richard D. Ernst<sup>b</sup>

<sup>a</sup>Department of Chemical Engineering  
Auburn University, Auburn, AL, 36849-5127

<sup>b</sup>Department of Chemistry  
University of Utah, Salt Lake City, UT, 84112-0850

## Introduction

The recent spike in energy prices has renewed attention on the production of chemicals from sources other than petroleum and focused attention on fossil fuels which are currently not recovered. In this light the use of SAPO catalysts in converting syngas either directly or indirectly to chemicals e. g. C<sub>2</sub>-C<sub>4</sub> olefins, is of interest. The main feedstock of current interest is remote or flared natural gas, although any feedstock convertible to syngas is technically viable. This means that coal and biomass are potential resources for chemicals currently produced from petroleum. We are especially interested in C<sub>2</sub>-C<sub>4</sub> olefins.

Flanigan, et al. have presented many of the most important properties of the SAPO catalysts in their foundational work<sup>1</sup>. A good review of the chemistry of methanol to hydrocarbons is presented by Stocker<sup>2</sup>. In his review it is noted that the pathway for methanol to olefins (MTO) is via a consecutive reaction with the dimethyl ether (DME) intermediate.

Many parameters such as acidity, pore size, composition, and method of preparation influence the activity of SAPO catalysts. Thus a particular SAPO, e. g., SAPO-34, may behave differently depending on its history and manner of preparation. A main obstacle in the MTO process is the rapid deactivation of the catalysts due to coke formation; however, regeneration is possible by oxidation as in a recirculating fluid bed. Here we have studied the effect of particle size on the activity, selectivity and lifetime of several small pore SAPO catalysts in the MTO reaction. Particle size variation was accomplished by grinding. It is possible that grinding could induce changes in the crystalline structure of the catalysts, however, this was not determined in our study, the main focus being on the particle size variations and the resulting reaction effects. A few other studies have examined the effects of particle size on this reaction<sup>3,4</sup>. We also report preliminary results on the effect of Ru incorporation on SAPO performance.

## Experimental

The original SAPO catalysts used in our present work were samples prepared previously in our laboratory by Adekkanattu<sup>5-8</sup>. Studies were performed on SAPO-34, 44, 47, and 56. Original samples were ground in a Wig-L-Bug (Dentsply/Rinn) grinder with agate vial and ball for various times. Particle size was examined by SEM before and after grinding.

MTO reactions were performed at 1 atm in a quartz tube fixed bed, generally at 400 °C, using 0.3 g catalyst and 0.003 ml/min liquid methanol vaporized into nitrogen at 36 ml/min. (WHSV = 0.5 hr<sup>-1</sup>). In addition to particle size, effects of temperature and incorporation of Ru were also studied<sup>9</sup>. Products were analyzed by GC with FID and Plot-Q capillary column. More details are provided in the thesis by Jean<sup>10</sup>.

## Results and Discussion

**Figure 1** shows SEM micrographs of (a) the original SAPO-44 particles and (b) after grinding for 15 min. The reduction in particle size is fairly obvious from the scales on the figures, although some of the finer particles tend to form agglomerates. **Figures 2** (a) and (b) show the product distribution from MTO reactions over these SAPO-44 particles. We see that the ground particles have longer lifetimes, having increased from *ca.* 4 hrs to 10 hrs for the production of C<sub>2</sub>-C<sub>4</sub> olefins. The selectivity of ethylene to propylene is not appreciably altered by the size reduction, however a notable change in selectivity to DME is apparent, as a result of the grinding. This latter finding is in keeping with the product distribution expected from particle size reduction in a diffusion controlled reaction with DME intermediate, i. e., an increase in selectivity of the intermediate due to lower intraparticle diffusional resistance<sup>11</sup>. As shown in **Figure 3**, similar results were obtained at 5 and 10 min grinding times, although particle sizes at lesser grinding times as viewed by SEM were not dramatically different from **Figure 1**(b). Similar changes in catalyst lifetime and DME selectivity, though not as large, were found in the performance of SAPO-34, 47, and 56. In a few cases, the grinding process caused a decrease in activity. An attempt to restore the activity of a spent SAPO-56 sample was unsuccessful, perhaps indicating the deactivation process, e. g., coke deposition, was uniformly spread throughout the particles, as opposed to being preferentially located around the external surface.

**Figure 4** shows the performance of Ru-SAPO-44. Comparison with the unmodified catalyst in **Figure 2**(a) shows a small improvement, *ca.* 1 hr, in C<sub>2</sub>-C<sub>4</sub> olefins based lifetime. Ru-SAPO-56 was also slightly improved, while, SAPO-34 was not improved by the Ru addition. These results are interesting, however, more work would be required, perhaps with other metals and conditions to fully determine the benefits of metals addition to the SAPOs.

## Conclusions

Particle size reduction shows potential as an effective way to increase lifetime of SAPO catalysts based on C<sub>2</sub>-C<sub>4</sub> olefins production, although for a completely deactivated catalyst grinding alone will not regenerate the catalyst. The selectivity of the intermediate DME is increased by particle size reduction in keeping with diffusional effects on selectivity of an intermediate in a series reaction pathway. Ru addition had only a small effect on the SAPO lifetimes in this limited study.

**Acknowledgment.** This research was supported by the U.S. Department of Energy Office of Fossil Energy, National Energy Technology Laboratory (NETL), under DOE Contract DE-FC26-02NT41594. The authors wish to acknowledge Dr. P. M. Adekkanattu for preparing the original SAPO catalysts.

## References

1. Flanigan, E. M., Lok, B. M., Patton, R. L. and Wilson, S. T.: *Proc. 7<sup>th</sup>. Int. Zeolite Conf.*, Tokyo, 103, **1986**.
2. Stocker, M., *Microporous and Mesoporous Materials* 29, **1999**, 3 – 48.
3. Chen, D., Kjell, M. Fuglerud, T., Holmen, A., *ibid.*, 191.
4. Dahl, I. M. Wendelbo, R., Andersen, A., Akporiaye, D. Mostad, H. Fuglerud, T., *ibid.*, 159.
5. Annual Report for Period May 2001- May 2002, DOE Cooperative Agreement No. DE-FC26-99FT40540, Prepared by Consortium for Fossil

- Fuel Science, University of Kentucky.
- Annual Report for Period May 2002- May 2003, DOE Cooperative Agreement No. DE-FC26-02NT41594, Prepared by Consortium for Fossil Fuel Science, University of Kentucky.
  - Obrzut, D.L., Adekkanattu, P. M., Thundimadathil, J., Liu, J., Dubois, D.R., Guin, J.A., *React. Kin. Catal. Lett.*, 80(1) **2003** 113.
  - Dubois, D.R., Obrzut, D.L., Liu, J., Thundimadathil, J., Adekkanattu, P. M., Guin, J. A., Punnose, A. Seehra, M. S., *Fuel Proc. Technol.*, 83(1-3), **2003**, 203.
  - Wilson, D.R., Stahl, L., Ernst, R. D., *Organometallic Synthesis*, 3, **1986**, 136.
  - Jean, L., M. S. Thesis, Auburn University, **2005**.
  - Petersen, E. E., *Chemical Reaction Analysis*, Prentice Hall, **1965**, p. 97.

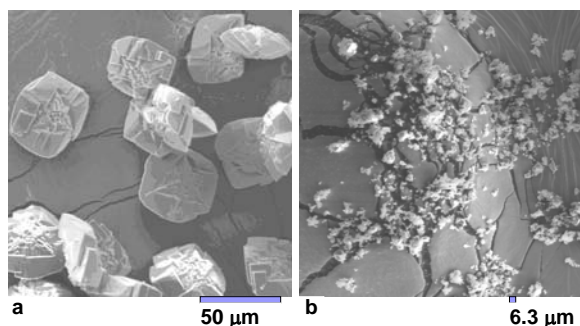


**Figure 1.** (a) SAPO-44 (Original Particles)  
(b) SAPO-44 (After 15 min Grinding)

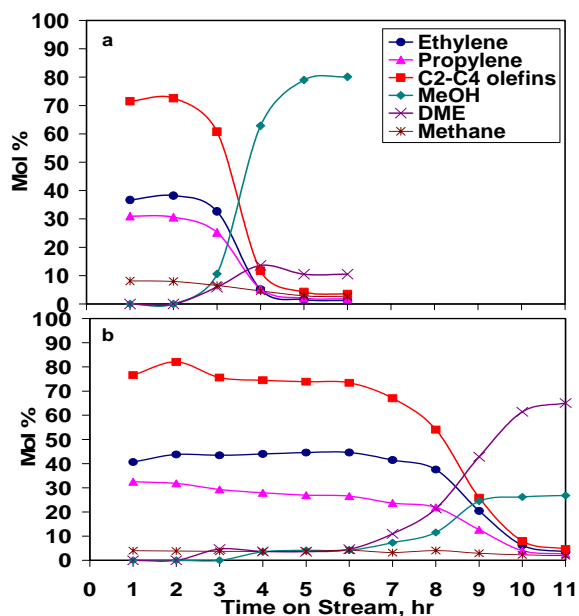


**Figure 2.** Product Distribution over: (a) Original Particles; (b) Ground Particles.

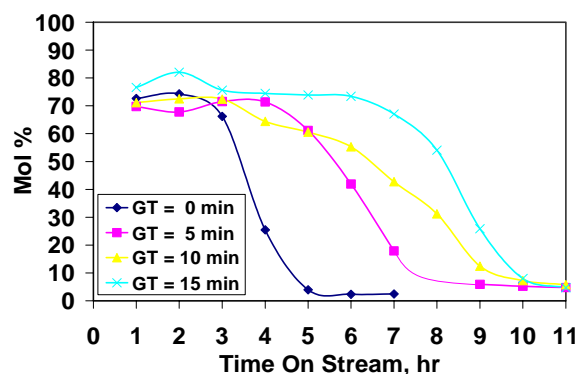


**Figure 3.** Effect of Grinding Time (GT) on C<sub>2</sub> - C<sub>4</sub> Olefins Production over SAPO-44.

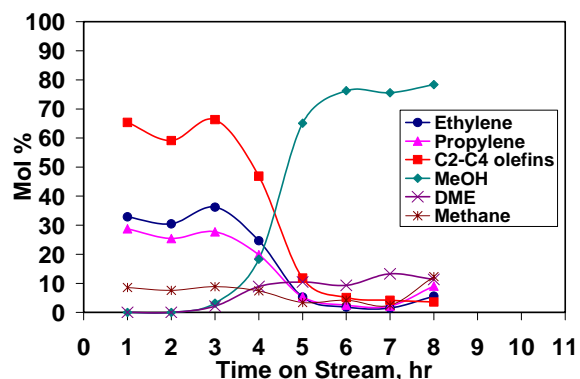


**Figure 4.** Product Distribution over Ru-SAPO-44.

# STABILITY AND STRUCTURE OF COBALT CATALYTIC SYSTEMS IN FISCHER-TROPSCH SYNTHESIS: SUPERCRITICAL FLUID MEDIA VERSUS CONVENTIONAL GAS-PHASE MEDIA

N. O. Elbashir<sup>a</sup>, P. Dutta<sup>b</sup>, M. S. Seehra<sup>b</sup>, C. B. Roberts<sup>a</sup>

<sup>a</sup>Department of Chemical Engineering, Auburn University, AL 36849,

<sup>b</sup>Physics Department, West Virginia University, Morgantown, WV 26506

## 1. Introduction

The limitations of the conventional media (gas-phase and liquid-phase) for Fischer-Tropsch synthesis (FTS) have driven research towards the application of supercritical fluid (SCF) solvents. The objective is to improve product control in the liquid fuels range and provide an opportunity for selective control of hydrocarbon distribution. The advantages of utilizing SCF solvents in the FTS reaction can be attributed to the fact that they offer high diffusivities (relative to a liquid phase FTS) and high solubilities and improved heat transfer (relative to a gas phase FTS). Utilization of cobalt-based catalysts in the FTS is known to provide the best compromise between performance and cost for the synthesis of hydrocarbons from syngas. Cobalt catalysts were also found to give the highest yields and longest lifetime producing mainly linear alkanes (paraffins)<sup>1</sup>. Since cobalt catalysts are not inhibited by the water-gas-shift (WGS), they give high productivity at high syngas conversion<sup>2</sup>. The efficiency of the synthesis process is critically dependent on the effectiveness and the stability of the cobalt catalyst. Most of the industrial cobalt-based systems used in the FTS reaction are either alumina supported or silica supported catalysts. Therefore, cobalt dispersion on the supported catalyst surface<sup>3</sup> and the interaction of the Co with the metal oxide support (which affects the electronic density as well as the structure of the metal crystallites<sup>4</sup>) are assumed to play significant roles in the catalyst performance measured by the hydrocarbon selectivity (C<sub>5+</sub>) and the catalyst activity.

The stability of the cobalt catalyst structure represents a major challenge to commercial-scale plants. The catalyst cost in addition to its regeneration cost represents a considerable proportion of the overall process cost. In many cases the cost of regenerating the catalyst is more expensive than the fresh catalyst cost<sup>5</sup>. Deactivation of the catalyst was assumed to be due to carbonaceous formations (specifically crystalline carbides) in the catalyst surface<sup>6</sup>, and also as a result of re-oxidation by the by-product water<sup>7</sup>.

Several techniques (XRD, magnetization, and electron magnetic resonance) were used to characterize our catalysts to determine the surface structure of the catalyst and the electronic states (Co<sup>0</sup>, CoO, Co<sub>3</sub>O<sub>4</sub>, Co<sup>2+</sup>) before and after the reaction. Our objective is to study the sensitivity of the supported-cobalt catalyst structure (physico-chemical characteristics, oxidation states, and crystalline structure of the active phase) during the FTS reaction. In general, it has been shown that supercritical phase FTS results in better catalyst stability at long time-on-stream (TOS) compared to conventional gas-phase FTS.

## 2. Experimental

**2.1 Catalysts.** Three catalytic systems were tested under both conventional gas-phase and supercritical phase FTS (15% Co/SiO<sub>2</sub> HSA supported on high surface area silica, 15% Co/SiO<sub>2</sub> LSA supported on low surface area silica, and 15% Co/Al<sub>2</sub>O<sub>3</sub>). The two silica supported catalysts were prepared in our lab<sup>8</sup>. The alumina

catalyst is a commercial catalyst purchased from United Catalyst Co. The silica supported catalysts were reduced in hydrogen environment, while the alumina supported catalyst was reduced in carbon monoxide environment.

**2.2 Catalyst Characterizations.** Room temperature X-ray diffraction (XRD) patterns of these catalysts were obtained with a Rigaku diffractometer using CuK<sub>α</sub> radiation with  $\lambda = 0.15418$  nm. Measurements of magnetization *M* versus temperature *T* and magnetic field *H* were done with a commercial SQUID (superconducting quantum interference device) magnetometer. Electron magnetic resonance (EMR) studies were carried out at the X-band frequency of 9.278 GHz with a variable temperature cryostat from Oxford Instruments. In this system, the microwave cavity remains at room temperature whereas the sample temperature can be varied from 4 K to 300 K. In the EMR resonance condition  $h\nu = g\mu_B H_0$ , the microwave frequency  $\nu$  is accurately measured by a frequency counter and the resonance field *H*<sub>0</sub> by a NMR probe. The magnetic field is modulated at 100 kHz so that the experimental traces represent d*P*/d*H* versus *H*, with *P* being the power absorbed. The back ground for the magnetic theory and the interpretation of the magnetic data was discussed in some detail in our previous study<sup>8</sup>.

**2.3 Fischer-Tropsch Studies.** The FTS reaction was carried out in a high-pressure FTS unit. A detailed description of this unit has been given elsewhere<sup>9</sup>. Hexanes (HPLC grade purchased from Fishers Co.) was used as the solvent for the supercritical phase FTS studies. The molar ratio between hexanes/syngas was kept at 3/1 whereby the syngas (H<sub>2</sub>/CO = 1) flows was at a rate of 50 sccm/g<sub>cat</sub>. In this study we referred to the supercritical hexanes FTS experiments as SCH-FTS.

Analysis of reactants and products was carried out by two online GCs. The results from the two GCs were used for conversion and selectivity calculations. A Varian 3300 GC with capillary column (DB-5) and a FID detector was used for the analysis of C<sub>2</sub>-C<sub>40</sub> hydrocarbons and oxygenates. Analysis of permanent gases (H<sub>2</sub>, CO, N<sub>2</sub>, CH<sub>4</sub>, CO<sub>2</sub>, C<sub>2</sub>H<sub>4</sub>, and C<sub>2</sub>H<sub>6</sub>) was conducted by a Varian CP-3800 GC with a packed column (Hayesep-DB100/120) and TCD detector. The online injection of our samples to the two GCs was carried out by two automated six-way-valves. Quantitative analysis of the results from the Varian CP-3800 provided the necessary data for the calculations. Reactants conversion (CO conversion and H<sub>2</sub>+CO (syngas) conversion), CH<sub>4</sub> selectivity, CO<sub>2</sub> selectivity, and C<sub>2</sub> (ethane and ethylene) selectivities were calculated using the response factor of N<sub>2</sub> from the TCD analysis as a reference. On the other hand, hydrocarbon product distributions (i.e. C<sub>2</sub> to C<sub>30</sub> selectivity data) were determined from the FID and TCD analysis as described in detail elsewhere<sup>9</sup>.)

## 3. Results and Discussion

Table 1 shows a summary of our catalyst XRD and EMR characterizations before (fresh calcined catalyst) and after the reaction (used catalyst after either conventional gas-phase FTS or SCH-FTS). Detailed discussions on the characteristics of fresh catalyst were given elsewhere<sup>8</sup>. Summarizing the results of Table 1, we conclude that the LSA 15% Co/SiO<sub>2</sub> used sample (under gas-phase FTS condition) contains Co<sup>0</sup> only which is the product of the reduction of Co<sub>3</sub>O<sub>4</sub> in the calcined unused sample. In the HSA 15% Co/SiO<sub>2</sub> used sample under (SCH-FTS conditions), we observed Co<sup>0</sup>/CoO composite, the quantity of CoO being much less than that of Co<sup>0</sup>. Thus either the reduction of Co<sub>3</sub>O<sub>4</sub> to Co<sup>0</sup> is not complete since some CoO is observed or some oxidation of Co<sup>0</sup> to CoO has taken place subsequent to the FTS experiments because of the high surface area of the catalysts.

**Table 1. Summary of the XRD and EMR characterization of the used cobalt-based catalytic systems under both gas-phase FTS and SCH-FTS.**

	XRD & EMR Characterizations	
	Fresh	Used
<b>Silica Catalysts</b>		
HSA 15%Co/SiO <sub>2</sub> (Used 10 days in gas-phase)	SiO <sub>2</sub> , Co <sub>3</sub> O <sub>4</sub>	SiO <sub>2</sub> (quartz, cristobalite, tridymite)
LSA 15%Co/SiO <sub>2</sub> (Used 13 days in SCH-FTS)	SiO <sub>2</sub> , Co <sub>3</sub> O <sub>4</sub> , Co <sup>2+</sup>	fcc-Co <sup>0</sup> , CoO, Co <sub>3</sub> O <sub>4</sub> (small) SiO <sub>2</sub> (cristobalite)
<b>Alumina Catalysts</b>		
15%Co/Al <sub>2</sub> O <sub>3</sub> (Unused, reduced catalyst)	Co <sub>3</sub> O <sub>4</sub> ; $\gamma$ -Al <sub>2</sub> O <sub>3</sub> $\epsilon$ -Al <sub>2</sub> O <sub>3</sub> CoO, hcp Co <sup>0</sup>	—
15%Co/Al <sub>2</sub> O <sub>3</sub> (Used 13 days in SCH-FTS)	Co <sub>3</sub> O <sub>4</sub> , $\delta$ -Al <sub>2</sub> O <sub>3</sub> , Co <sup>2+</sup>	hcp-Co <sup>0</sup> , CoO, Co <sub>3</sub> O <sub>4</sub> ; $\gamma$ -Al <sub>2</sub> O <sub>3</sub> , $\epsilon$ -Al <sub>2</sub> O <sub>3</sub>
15%Co/Al <sub>2</sub> O <sub>3</sub> (Used 7 days in gas-phase-FTS)	Co <sub>3</sub> O <sub>4</sub> , $\delta$ -Al <sub>2</sub> O <sub>3</sub> , Co <sup>2+</sup>	hcp-Co <sup>0</sup> , fcc-Co <sup>0</sup> , Co <sup>0</sup> , $\gamma$ -Al <sub>2</sub> O <sub>3</sub>

Three samples of the alumina supported catalysts were characterized; (1) unused 15% Co/Al<sub>2</sub>O<sub>3</sub> which was reduced in CO environment.; (2) used sample of 15% Co/Al<sub>2</sub>O<sub>3</sub> after SCH-FTS condition for 13 days; (3) used sample of 15% Co/Al<sub>2</sub>O<sub>3</sub> after gas-phase FTS for 7 days for temperatures up to 260°C. Partial reduction of the alumina supported catalyst in CO environment (the unused sample) prior to in situ reduction with the syngas during FTS allows us an opportunity to evaluate the extent of in situ reduction. Our XRD characterization of the unused alumina catalyst showed two Al<sub>2</sub>O<sub>3</sub> phases and Co<sub>3</sub>O<sub>4</sub> with only a hint of the presence of the hexagonal-close-packed (hcp) phase of Co<sup>0</sup>. For the used sample after supercritical phase operation the characterizations show presence of some CoO and hcp Co<sup>0</sup> and absence of Co<sub>3</sub>O<sub>4</sub>. Thus reduction of Co<sub>3</sub>O<sub>4</sub> to CoO and hcp Co<sup>0</sup> has occurred. For the used sample from gas-phase FTS both fcc Co<sup>0</sup> and hcp Co<sup>0</sup> are present. Thus the reduction of Co<sub>3</sub>O<sub>4</sub> to Co<sup>0</sup> is complete for that sample. The particle sizes of Co<sup>0</sup> determined from the width of the XRD peaks are 13 nm for fcc Co<sup>0</sup> and 14 nm for hcp Co<sup>0</sup>.

Figs. 1 and 2 show an example of stability tests on the alumina-supported catalyst (15% Co/Al<sub>2</sub>O<sub>3</sub>) under different reaction conditions in the SCH-FTS and gas phase-FTS reactions at relatively long TOS. Syngas conversion is used to represent the activity of the catalyst. During the SCH-FTS testing, the catalyst showed good stability in syngas conversion (~80%) at 240 °C and 60 bar. The temperature was then decreased to 230 °C, while the pressure was kept constant at 60 bar. As a result, syngas conversion decreased to ~58%. A stable trend was observed under these conditions for more than 48 hrs TOS. The stability test was then followed by increasing the temperature to 250 °C and the pressure to 65 bar. At these conditions, syngas conversion reaches its highest level, 93%, at the initial 2 hrs TOS and then declined to ~87% for more than 100 hrs

TOS. The aforementioned conditions were selected based on our previous investigations of the alumina-supported catalyst, whereby an optimum performance in both activity and selectivity was observed<sup>9</sup>. Upon returning to the initial conditions (240 °C and 60 bar), no significant changes in either syngas conversions was observed as shown in Fig.1.

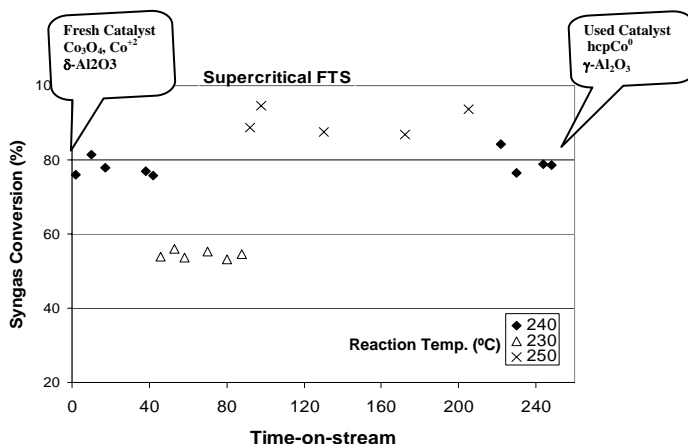


**Figure 1.** Stability of the 15% Co/Al<sub>2</sub>O<sub>3</sub> catalyst activity (syngas conversion (%)) with TOS in SCH-FTS at different reaction conditions (240 °C and 60 bar; 230 °C and 60 bar; 250 °C and 65 bar; and 240 °C and 60 bar). P<sub>syngas</sub> = 20 bar, syngas flowrate 50 sccm/g<sub>cat</sub>, and hexane/syngas molar ratio is 3.

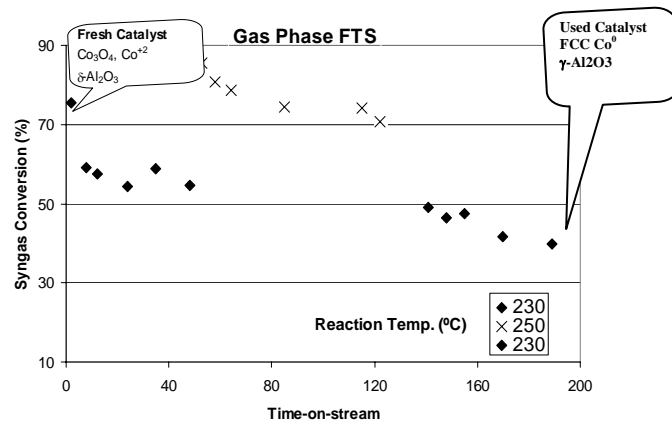


**Figure 2.** Stability of the 15% Co/Al<sub>2</sub>O<sub>3</sub> catalyst activity (syngas conversion (%)) with TOS in gas phase-FTS at different reaction conditions (230 °C and 20 bar; 250 °C and 20 bar; and 230 °C and 20 bar). P<sub>syngas</sub> = 20 bar, syngas flowrate 50 sccm/g<sub>cat</sub>.

In the gas phase-FTS (Fig.2), the stability test was initialized at 230 °C and 20 bar for 50 hrs TOS. The catalyst reached a steady value of activity within 10 h of ~59% syngas conversion. Upon increasing the temperature to 250 °C, significant increase in syngas conversion (~88%) was obtained during the first 7 hrs. However, as the TOS was increased (up to 45 h) the syngas conversion decreased to reach 74%. The activity reached a steady value after 70 hrs TOS under the above conditions. Returning to the low temperature conditions (230 °C) resulted in a significant drop (c.a. 25%) in syngas conversion.

In order to understand the role of the reaction media on the catalyst structure and activity we conducted a correlation between the stability tests and the used catalyst characteristics. As discussed earlier our findings show that the dominant cobalt phase of the used sample from SCH-FTS is hcp Co<sup>0</sup>, whereas, the dominant phase in the used sample from gas-phase FTS is fcc Co<sup>0</sup>. It is noteworthy to mention here that the fcc Co<sup>0</sup> was not detected in the reduced catalyst before the reaction (reduced-unused 15% Co/Al<sub>2</sub>O<sub>3</sub>). This suggests that the in situ reduction during the SCH-FTS stabilizes the hcp Co<sup>0</sup> form, which has more surface defects (corners and edges) in the metallic phase than the cubic phase one (fcc Co<sup>0</sup>). In a previous study, Rathousky, et al. stated that the metallic cobalt formed on the outer surface of the CoO crystal-lines enhances the adsorption centers of weakly bonded carbon monoxide molecules<sup>14</sup>. Another reason that may contribute to the stability in the catalyst activity in the SCH media is the good temperature distribution inside the fixed-bed-reactor compared to the poor one in the gas-phase media<sup>16</sup>. The control of temperature distribution in the reduction process is known to avoid the increase of cobalt-support interactions and agglomerations of cobalt nano-particles<sup>10</sup>. Our results shows that there is no significant difference between cobalt particle size of the unused catalyst and that of used catalyst from SCH-FTS (both have size >12 nm)<sup>17</sup>. Small particles could easily be reoxidized by water and other reaction conditions during the FTS reaction.

The used silica-supported catalysts showed different characteristics from that of the alumina supported ones. The XRD characterizations of the silica supported catalyst (Table 1) show the presence of quartz, cristobalite, and tridymite silicate forms; however, minimal amounts were detected in SCH-FTS used catalyst. It is also important to mention that no Co<sup>0</sup>, CoO, Co<sub>3</sub>O<sub>4</sub> XRD pattern was observed in the used catalyst from the gas-phase where only silicate forms were detected. This suggests that the in situ reduction of the catalyst during the gas-phase FTS is minimal. The presence of the silicate forms in the two used catalysts suggests that the in situ reduction during the FTS reaction is different from that in the alumina-supported catalyst.

#### 4. Conclusions

Our XRD and magnetic characterizations of the used catalysts show that in situ reducibility of the cobalt oxide takes place during the FTS reaction in both gas-phase FTS and SCH-FTS conditions. In the latter, the in situ reduction of Co<sub>3</sub>O<sub>4</sub> gave active crystal-lines of hcp and fcc Co<sup>0</sup> that were found to be very stable for a long TOS. As a result, the activity and selectivity of the catalyst in the SCH medium is more stable and recoverable than that under gas-phase FTS conditions. Our findings also show that the in situ reduction pathway of the silica supported catalyst is different than that of the alumina supported one; however, a stable form of fcc Co<sup>0</sup> has also been detected on the used catalyst from the SCH-FTS operation. Detailed discussions on the influence of the catalyst surface characteristics on both the activity and selectivity of the FTS reaction in both gas-phase and SCH phase were covered elsewhere<sup>17</sup>.

**Acknowledgments.** The authors would like to acknowledge the financial support of the Consortium for Fossil Fuel Science (under the Department of Energy Grant DE-FC26-02NT41594) and by Nippon Oil Corporation, Japan (CBR and NOE).

#### References

- (1) Chaumette, P.; Verdon, C.; Boucot, P. *Topics in Catalysis* **1995**, 2, 301-311.
- (2) Van Berge, P. J.; Everson, R. C. *Studies in Surface Science and Catalysis (Natural Gas Conversion IV)* **1997**, 107, 207-212.
- (3) Tauster, S. J.; Fung, S. C. *J. Catal.* **1978**, 55, 29.
- (4) Iglesia, E.; Soled, S. L.; Fiato, R. A. *J. Catal.* **1992**, 137, 212-224.
- (5) Zhan, X.; Arcuri, K.; Huang, R.; Agee K; Engman, J.; Robota, H. J. *Prep. Pap.-Am. Chem. Soc., Div. Pet. Chem.* **2004**, 49, 179.
- (6) Gruver, V.; Zhan, X.; Engman, J.; Robota, H. J. *Prep. Pap.-Am. Chem. Soc., Div. Pet. Chem.* **2004**, 49, 192-194.
- (7) Li, J.; Jacobs, G.; Das, T.; Zhang, Y.; Davis, B. *App. Catal. A: Gen.* **2002**, 236, 67-76.
- (8) Dutta, P.; Elbashir, N. O.; Manivannan, A.; Seehra, M. S.; Roberts, C. B. *Catal. Letters* **2004**, 98, 203-210.
- (9) Elbashir, N. O.; Roberts, C. B. *Ind. Eng. Chem. Res.* **2005**, 44, 505-521.
- (10) Khodakov, A. Y.; Griboval-Constant, A.; Bechara, R.; Zholobenko, V. L. *J. Catal.* **2002**, 206, 230-241.
- (11) Iglesia, E.; Reyes, S. C.; Madon, R. J.; Soled, S. L. *Adv. Catal.* **1993**, 39, 221-302.
- (12) Reuel, R. C.; Bartholomew, C. H. *J. Catal.* **1984**, 85, 78-88.
- (13) Elbashir, N. O.; Roberts, C. B. *Prep. Pap.-Am. Chem. Soc., Div. Pet. Chem.* **2004**, 49, 157-160.
- (14) Rathouský, J.; A., Z.; Lapidus, A.; Krylova, A. *App. Catal. A: Gen* **1991**, 79, 167-180.
- (15) Enache, D. I.; Rebours, B.; Roy-Auberger, M.; Revel, R. *J. Catal.* **2002**, 205, 346-353.
- (16) Yokota, K.; Hanakata, Y.; Fujimoto, K. *Chemical Engineering Science* **1990**, 45, 2743-2749.
- (17) Elbashir, N. O.; Dutta, P.; Manivannan, A.; Seehra, M. S.; Roberts, C. B. *App. Catal. A: Gen.* **2005**, 285, 169-180.

# CHAIN INITIATION OF FISCHER-TROPSCH WITH ACETYLENE INCORPORATION

Yulong Zhang, Li Hou, John W. Tierney and Irving Wender

Department of Chemical and Petroleum Engineering, University of Pittsburgh, Pennsylvania, USA

## Introduction

Fischer-Tropsch (F-T) synthesis converts syngas (CO and H<sub>2</sub>), which can be produced from coal, natural gas, biomass and any carbonaceous materials, into long chain hydrocarbons which can be transformed to fuels and chemicals. It is very attractive to nations who have abundant coal or natural gas but lack indigenous oil. The mechanism of the FT reaction is still under debate although it has been investigated for about 80 years. Major obstacles are to distinguish many complex intermediates formed during F-T reactions. Schulz<sup>1</sup> pointed out that the F-T regime is established during the synthesis by restructuring catalyst surface and suppressing of undesired reactions. F-T active sites are difficult to characterize spectroscopically under high vacuum conditions. Use of probe molecules has been shown to be an effective way to study the F-T mechanism<sup>2</sup>.

The F-T synthesis is a stepwise growth of hydrocarbon chains by addition of monomeric units. Unlike usual polymerization processes, the reaction proceeds by the addition of monomers formed in-situ from syngas. In previous studies, we found that long chain alkynes are incorporated more easily than corresponding alkenes<sup>3</sup>. It has been reported that ethylene is 10 to 40 times more easily incorporated into the F-T synthesis than are higher olefins. In this work acetylene is used as a probe molecule to study the mode of initiation of the F-T synthesis with consideration of possible differences in the pathways that occur with cobalt and iron catalysts.

## Experimental

Supported cobalt catalysts were prepared by incipient-wetness impregnation of cobalt nitrate on alumina. A precipitated iron catalyst with a composition of 100Fe/4.4Si/1.25K was obtained from Dr. B. Davis of the University of Kentucky.

The F-T reaction was carried out in a computer controlled fixed bed reactor (stainless-steel with i.d. 3/8 inches). Acetylene was introduced from a tank of premixed gas containing (mol): 1% acetylene, 10% Ar, 44% CO, and 45% H<sub>2</sub> obtained from Praxair. H<sub>2</sub> was added when the H<sub>2</sub>/CO ratio needs to be adjusted. Co catalysts were activated by H<sub>2</sub> at a rate of 50 ml/min, with a temperature program ramping from room temperature to 350°C at 1°C/min, holding at 350°C for 10 hours. Fe catalysts were activated similarly but kept at 350°C for 5 hours and 450°C for 2 hours. The F-T reaction was started by gradually increasing the CO and H<sub>2</sub> flow rate to avoid a temperature surge due to active sites present in the fresh catalysts. Products were analyzed by two online GCs (HP6890 and HP5890).

## Results and Discussion

Addition of acetylene on cobalt catalysts increases the yield of C<sub>2</sub><sup>+</sup> products up to about C<sub>10</sub>. It can be seen from Figure 1 that C<sub>3</sub> has a three fold increase upon addition of 1% acetylene. Compared to 1-hexyne, acetylene is 3 to 4 times easier to incorporate into the F-T products. A significant amount of acetylene is dimerized to C<sub>4</sub>. Dimerization is not a part of the F-T reaction since it is not sensitive to sulfur. C<sub>4</sub> products are mainly internal olefins; however, they are also capable of chain initiation. As with cofeeding internal acetylenes we have reported earlier<sup>3</sup>, isomers such as 2-methylbutane and 3-methylpentane are produced when acetylene is cofed.

One striking effect of cofeeding acetylene is initiation of the F-T chain growth at lower temperatures. At 120°C, appreciable amount of F-T products can still be obtained with cofeeding of 1% of acetylene, otherwise, the FT reaction has no activity at such a low temperature. Incorporation of acetylene on cobalt catalyst produces oxygenates; however, only C<sub>3</sub> oxygenates and a small amount of C<sub>5</sub> oxygenates are produced with cofeeding acetylene, apparently by hydroformylation of adsorbed unsaturated C<sub>2</sub> and C<sub>4</sub> species.

Acetylene can initiate FT on iron catalysts effectively; however, there are a number of differences between iron and cobalt catalysts. Only a small amount of dimerization was observed on iron catalysts. Instead of only one or two oxygenates as on cobalt catalysts, iron catalysts produces a spectrum of oxygenates which follows the Anderson-Schultz-Flory distribution as shown in Figure 2. Formation of oxygenates is an intrinsic property of iron catalysts.

Acetylenes initiate the chain but are not incorporated into the growing chain. The alpha value of the F-T reaction declines with cofed acetylene due to the increasing number of chain initiators. It is also evidenced by using phenylacetylenes as probes.

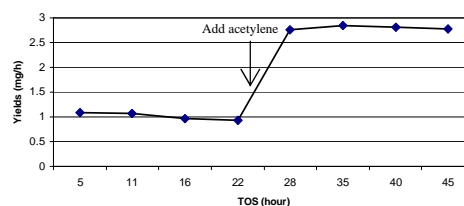


**Figure 1.** Yield of C<sub>3</sub> hydrocarbons with TOS on a cobalt catalyst (10Co/90Al<sub>2</sub>O<sub>3</sub>) at 100 psi., 180°C, H<sub>2</sub>/CO=1, 1% acetylene.

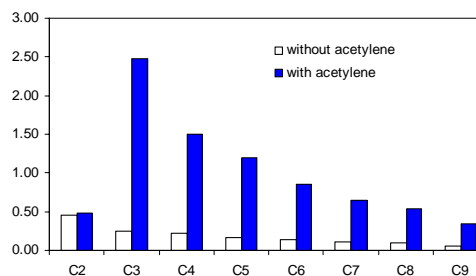


**Figure 2.** Oxygenated product distribution without/with acetylene incorporation on a iron catalyst (10Co/90Al<sub>2</sub>O<sub>3</sub>) at 300psi, 180°C, H<sub>2</sub>/CO=1, 1% acetylene.

## Conclusions

Acetylene is incorporated into the F-T reaction much more effectively than are higher acetylenes, a finding similar to results reported with olefin addition. Alpha values decreased upon addition of acetylene, indicating that acetylene, a two-carbon entity serves as a chain initiator. Oxygenates on cobalt catalysts is formed by hydroformylation while oxygenates are essential for chain growth on iron catalysts.

**Acknowledgement.** We thank the U.S. Department of Energy for financial support under grant No. DE FC26 99FT40540.

## References

- (1) Schulz, H.; Nie, Z. Q.; Ousmanov, F. *Catal. Today* **2002**, 71, 351-360.
- (2) Turner, M. L.; Marsih, N.; Mann, B. E.; Quyoum, R.; Long, H. C.; Maitlis, P. M. *J. Am. Chem. Soc.* **2002**, 124, 10456-10472.
- (3) Zhang, Y.; Hou, L.; Tierney, J. W.; Wender, I. *Top. Catal.* **2005**, 33.

# AEROGEL-SUPPORTED TRANSITION METAL CATALYSTS FOR FISCHER-TROPSCH AND RELATED REACTIONS

Gregory C. Turpin, Brian C. Dunn, Yifan Shi, Zhiru Ma, Ronald J. Pugmire, Edward M. Eyring, and Richard D. Ernst

Department of Chemistry, University of Utah Salt, Lake City, UT 84112

## Introduction

The Fischer-Tropsch and Water Gas Shift reactions each offer the potential for providing solutions to important future energy concerns. In each case, catalysts employed for these processes tend to be late transition metals deposited on typical supports such as silica, alumina, or titania. While numerous studies have addressed the roles played by various catalyst and support combinations, far less attention has been devoted to studies involving aerogel supports, whose highly porous natures should promote more effective catalyst dispersal and enhanced mass transport of reactant and product molecules through the aerogel pores.<sup>1</sup> Additionally, catalytic studies utilizing aerogel supports may be carried out either under gas-phase or supercritical conditions, leading to further control over the nature of the reaction.<sup>2</sup>

The unique structures and properties of aerogels allow for the preparation of very new catalyst/support motifs. In one application, the highly porous aerogel backbone can serve as a framework onto which a more desirable support material may be deposited. This approach could be advantageous in cases in which the more desirable support either may be costly, or does not form a reasonable aerogel structure on its own. As will be described, this approach has been successfully applied to the preparation of a ceria-coated silica aerogel. A second opportunity for aerogels relates to the catalyst incorporation step. Since partial wetting of an aerogel structure can lead to drastic collapse of the pore structure, gas-phase incorporation processes could offer some advantages, including the potential of effecting single site metal incorporation and of delivering one metal selectively to another on the support surface.

## Experimental

**Catalyst Supports.** Silica aerogels were prepared as previously described.<sup>3</sup> Solution phase loading of cerium(IV) alkoxides was accomplished by first replacing the solvents in a 10 mL solid monolithic alcogel sample through 4-5 equilibrations with 20-25 mL volumes of THF, after which the external solvent was replaced by a solution of the cerium alkoxide in THF. Subsequent equilibration led to an even distribution of cerium throughout the entire solution volume, within and outside of the alcogel. The alcogel monolith was then removed and subjected to two similar equilibrations with acetone, after which the monolith was placed in a CO<sub>2</sub> atmosphere, pressurized to supercritical conditions, and dried to form the aerogel.

**Catalyst Preparations.** The metal pentadienyl compounds were prepared according to literature methods.<sup>4-6</sup> For gas-phase incorporations of the transition metal complexes, the appropriate masses of organometallic compound and crushed aerogel were combined under nitrogen in a Schlenk tube which was then placed under static vacuum and rotated constantly until the separate organometallic phase was no longer visible. Oxygen gas was then passed over the doped aerogel, beginning at 25 °C, with the temperature thereafter slowly brought to 25-350 °C, depending on sample. Subsequently, the supported metal oxide was heated to 500 °C, and reduced in a hydrogen stream.

**Catalytic Studies.** Fischer-Tropsch reactions were carried out in a laboratory-scale packed bed reactor, as previously described,<sup>3</sup>

except that C<sub>1</sub>-C<sub>13</sub> hydrocarbon products were analyzed by gas chromatography on a capillary column (DB-5, 0.53 mm I.D. and 30 m length) with an FID.

## Results and Discussion

The high activities of copper-, gold-, and palladium-derived water gas shift catalysts supported on ceria<sup>7,8</sup> have led to an interest in examining their activities on aerogels. Unfortunately, ceria-based aerogels do not show the structural stability one finds for silica aerogels at higher temperatures.<sup>9</sup> To circumvent this problem, attempts to bind ceria on silica aerogels have been undertaken. The hydrolytically sensitive Ce(O-*i*-Pr)<sub>4</sub>(*i*-PrOH)<sup>10</sup> does in fact readily incorporate into highly porous silica aerogel via standard solution methods, after which other metals of interest, such as palladium, can be incorporated by gas-phase or solution methods.

Gas-phase incorporation of metals such as iron and ruthenium occurs surprisingly well using their relatively air- and water-stable M(2,4-C<sub>7</sub>H<sub>11</sub>)<sub>2</sub> or M(C<sub>5</sub>H<sub>5</sub>)(2,4-C<sub>7</sub>H<sub>11</sub>) compounds (C<sub>5</sub>H<sub>5</sub> = cyclopentadienyl; C<sub>7</sub>H<sub>11</sub> = dimethylpentadienyl). Incorporation is immediate, occurring via protonation of a 2,4-C<sub>7</sub>H<sub>11</sub> ligand. Similarly, Co(*c*-C<sub>8</sub>H<sub>13</sub>)(*c*-C<sub>8</sub>H<sub>12</sub>)<sup>11</sup> undergoes facile incorporation (*c*-C<sub>8</sub>H<sub>13</sub> = cyclooctenyl; *c*-C<sub>8</sub>H<sub>12</sub> = cyclooctadiene). Cobaltocene, Co(C<sub>5</sub>H<sub>5</sub>)<sub>2</sub>,<sup>12</sup> incorporates more slowly, yielding significant quantities of cyclopentene. Although spectroscopic data indicate that single-site incorporation is initially occurring for the metal under these conditions, agglomeration appears quite facile subsequent to oxidation. This, as well as the high reactivities of the aerogel surfaces with the metal pentadienyl complexes, appears to be a result of the aerogel surface providing a poorly coordinating environment.

Figures 1 and 2 present selectivity and activity results for a ruthenium catalyst prepared by gas-phase deposition onto a silica aerogel. The catalyst was examined for a total of 50 hours on stream and remained active until removed from the reactor. The time dependent activity of this sample is atypical and likely related to the calcination temperature.

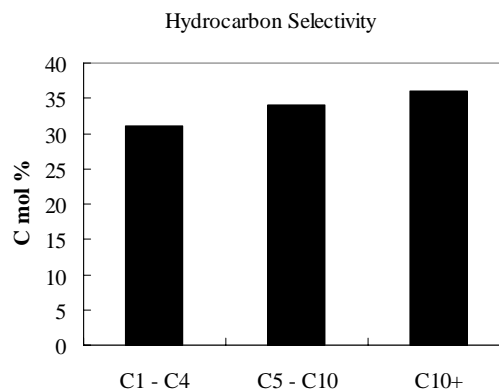


**Figure 1.** Hydrocarbon product distribution after 35 hours on stream from a 2% ruthenium catalyst supported on silica aerogel.

The gas-phase approach also allows for the selective delivery of one metal to another on a surface, via redox reactions. Thus, the 19 electron cobaltocene, which is a good reducing agent capable of reducing many metal oxides to the metals, should readily "target" a variety of unsupported oxides. Of particular interest for Fischer-Tropsch applications would be ruthenium. Initial results indicate that not only does cobaltocene incorporate more readily into oxidized

ruthenium-doped aerogels, but the resulting catalysts are more active than ones derived from less selective cobalt incorporations.

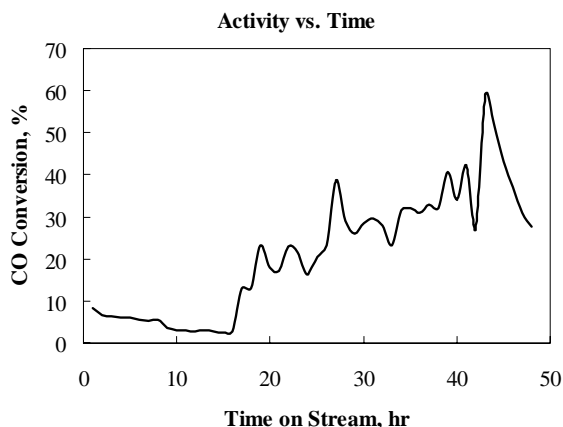


**Figure 2.** Carbon monoxide conversion as a function of time on stream for the 2% ruthenium catalyst.

### Conclusions

Silica aerogels have been found to exhibit unusually high reactivities toward some relatively unreactive organometallic compounds, thereby allowing for the facile incorporation of a variety of metals, and even the selective delivery of one metal to another on the surface. The resulting catalysts have shown interesting reactivity trends for the Fischer-Tropsch process. The highly porous and reactive aerogels also readily incorporate cerium(IV) alkoxides, and thereby offer substantial promise as scaffolds to support other, less robust supports.

**Acknowledgement.** The U.S. Department of Energy provided financial support to the Consortium for Fossil Fuel Science for this study (contract # DE-FC26-02NT41954).

### References

- (1) Husing, N.; Schubert, U. *Angew. Chem. Int. Ed.* **1998**, *37*, 22-45.
- (2) Elbashir, N.O.; Roberts, C.B. *Ind. Eng. Chem. Res.* **2005**, *44*, 505-521.
- (3) Dunn, B. C.; Cole, P.; Turpin, G. C.; Ma, Z.; Pugmire, R. J.; Ernst, R. D.; Eyring, E. M.; Shah, N.; Huffman, G. P. Preprints of Symposia - American Chemical Society, Division of Fuel Chemistry **2004**, *449(1)*, 329-330.
- (4) Wilson, D.R.; Stahl, L.; Ernst, R.D. *Organometallic Syntheses* **1986**, *3*, 136-141.
- (5) Elschenbroich, C.; Bilger, E.; Ernst, R.D.; Wilson, D.R.; Kralik, M.S. *Organometallics* **1985**, *4*, 2068-2071.
- (6) Gleiter, R.; Hyla-Kryspin, I.; Ziegler, M.L.; Sergeson, G.; Green, J.C.; Stahl, L.; Ernst, R.D. *Organometallics* **1989**, *8*, 298-306.
- (7) Fu, Q.; Saltsburg, H.; Flytzani-Stephanopoulos, M. *Science* **2003**, *301*, 935-938.
- (8) Qi, X.; Flytzani-Stephanopoulos, M. *Ind. Eng. Chem. Res.* **2004**, *43*, 3055-3062.
- (9) Thundathil, M.A.; Lai, W.; Noailles, L.; Dunn, B.S.; Haile, S.M. *J. Am. Ceram. Soc.* **2004**, *87*, 1442-1445.
- (10) Vaartstra, B.A.; Huffman, J.C.; Gradeff, P.S.; Hubert-Pfalzgraf, L.G.; Daran, J.-C.; Parraud, S.; Yunlu, K.; Caulton, K.G. *Inorg. Chem.* **1990**, *29*, 3126-3131.
- (11) Dumestre, F.; Chaudret, B.; Amiens, C.; Fromen, M.-C.; Casanove, M.-J.; Renaud, P.; Zurcher, P. *Angew. Chem. Int. Ed.* **2002**, *41*, 4286-4289.
- (12) Eisch, J.J.; King, R.B. *Organometallic Syntheses* **1965**, *1*, 70-71.

# HYDROGEN PRODUCTION FROM METHANOL IN SUPERCRITICAL WATER

Jayant B. Gadhe and Ram B. Gupta

Department of Chemical Engineering  
Auburn University  
Auburn, AL 36849-5127.

## Introduction

The development of proton exchange membrane fuel cells for various transportation applications has resulted in a need of on-board and stationary reformers which can supply high purity hydrogen at low cost. Designing a process to produce  $H_2$  at a very high pressure is an attractive approach for mobile and portable applications owing to its low storage volume. The reforming of hydrocarbons can be carried out in the presence of supercritical water instead of steam as used in the conventional processes, to produce  $H_2$  at a very high pressure.

There are several advantages of carrying out the reforming reactions in supercritical water over the conventional processes. The density of supercritical water is higher than that of steam which results in a high space-time yield and the higher values of thermal conductivity and specific heat of supercritical water are beneficial for the endothermic reforming reaction.  $H_2$  is available at a high pressure which can be stored directly, thus avoiding the problems associated with its compression. The process becomes economical as the compression work is reduced owing to the low compressibility of liquid feed as compared to that of gaseous  $H_2$ .<sup>1</sup> Hydrocarbons are completely soluble in supercritical water which minimizes the formation of char or slag which may otherwise cause catalyst deactivation. This is particularly important in the generation of  $H_2$  from heavy oils such as diesel. The generation of  $H_2$  by the steam reforming of biomass leads to the formation of significant amounts of tar and char which limits the yield of  $H_2$  and the gaseous product contains higher hydrocarbons in addition to the desired light gases. Researchers have carried out the catalytic gasification of biomass or its model compounds in supercritical water to produce  $H_2$ -rich gas with effectively no tar or char formation.<sup>2</sup>

Methanol is chosen as feedstock for reforming because of its high hydrogen-to-carbon ratio and absence of carbon-carbon bonds. It is in the liquid state under normal conditions and hence can be stored and pumped easily. The major reactions involved in the methanol reforming are:



To study the impact of pressure on the  $H_2$  yield, equilibrium calculations were performed using Gibbs free energy minimization method and Peng-Robinson equation of state. **Figure 1** shows that as pressure increases, there is an increase in the  $CH_4$  moles and decrease in the  $H_2$ ,  $CO$  and  $CO_2$  moles. It suggests that methanation of  $CO$  (reaction 3) and  $CO_2$  (reaction 4) is favored at higher pressures. Methanation of  $CO$  results in a loss of 3 moles of  $H_2$  while methanation of  $CO_2$  results in a loss of 4 moles of  $H_2$ . To enjoy the benefits of the reforming of methanol in supercritical water which are mentioned before, it becomes important to prevent the loss of  $H_2$  by minimizing the methanation reactions.

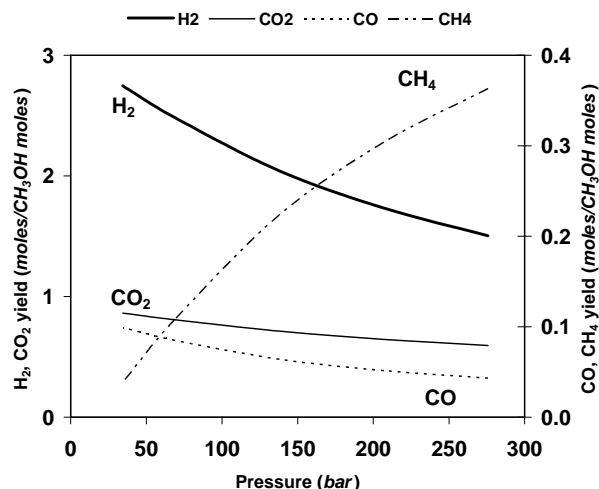


**Figure 1.** Dependence of gas yield on pressure using ASPEN+ equilibrium calculations. (10 wt.% methanol, 700 °C)

## Experimental

**Materials.** Methanol (99.9%), KOH (88.7% assay) and  $K_2CO_3 \cdot 1\frac{1}{2}H_2O$  (99.9% assay) were obtained from Fisher.

**Apparatus.** **Figure 2** shows schematic of the apparatus used in the study. A tubular reactor made of Inconel 600 (Microgroup) having a composition of 73% Ni, 18% Cr, 9% Fe was used. The reactor wall provides the catalytic surface area for the reactions. Later the reactor was replaced with a Ni-Cu tubing (Supelco) having a composition of 67% Ni, 33% Cu.

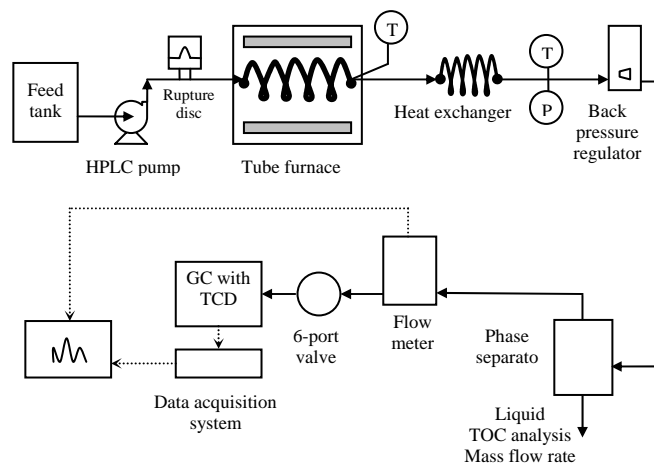


**Figure 2.** Schematic of the experimental setup used for methanol reforming in supercritical water.

Aqueous methanol from the feed tank was pumped to the reactor using an HPLC pump (Waters 590). The reactor was heated using a tube furnace equipped with a temperature controller (Thermolyne 21100). The gas mixture exiting the reactor was cooled using an air-cooled heat exchanger made of SS 316 tubing. Pressure was measured by a pressure gauge P. The pressure was let down to the ambient by means of a back pressure regulator (Straval). The gas-liquid mixture was separated in a glass phase separator having gas tight valves to prevent the escape of gases. The gas flow rate was measured using a gas flow meter (Omega FMA-1600). A six-port

injection valve (Valco) having a 100  $\mu\text{L}$  sample loop was used for the online sample injection. The gas composition was measured using a gas chromatograph (Varian 3700) equipped with a TCD and 60/80 Carboxen-1000 carbon molecular sieve column. (Supelco) The mass flow rate of the liquid coming out of the phase separator was measured using a balance. The total organic carbon (TOC) content of the liquid was analyzed using a TOC analyzer (OI Analytical Model 700).

## Results and Discussion

**Figure 3** shows that as pressure is raised from 34 to 276 bar, the  $\text{H}_2$ , CO and  $\text{CO}_2$  moles decrease while the  $\text{CH}_4$  moles increase as anticipated, suggesting that the methanation reactions, of both CO and  $\text{CO}_2$  are favored at the higher pressures. The  $\text{H}_2$  yield ( $\text{H}_2$  moles/ $\text{CH}_3\text{OH}$  moles) has dropped from 2.75 at 34 bar to 1.50 at 276 bar. The increase in density at the higher pressures leads to an increase in the residence time which ranged from 7 seconds at 34 bar to 59 seconds at 276 bar which resulted in the near-equilibrium yields.

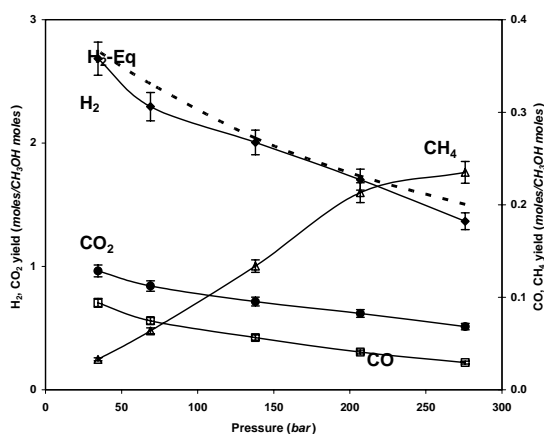
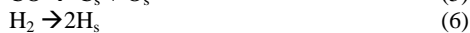


**Figure 3.** Effect of pressure on gas yield. (10 wt.% methanol, 0.5 mL/min, 700 °C, reactor length = 2 m)

The pressure variation was studied again in the Ni-Cu reactor at a lower residence time. **Figure 4** shows that the increase in pressure has a very little effect on the gas yields in this case. The  $\text{H}_2$  yields which are higher than the equilibrium  $\text{H}_2$  yields, remain fairly constant over the entire pressure range. The  $\text{CH}_4$  yield is found to be almost negligible. This could be the combined effect of the low residence time, which ranged from 2 seconds to 17 seconds in this case and possibly the catalytic activity of the Ni-Cu reactor.

This behavior of the Ni-Cu reactor can be explained based on the mechanism of CO methanation. It proceeds via dissociative chemisorption of CO and  $\text{H}_2$  to form intermediates which combine to form  $\text{CH}_4$  as shown in reactions 5 to 7.



Alloying Ni with Cu results in the dilution of active Ni in an inactive matrix which diminishes the number and size of Ni clusters which are necessary for the dissociation of CO and deposition of  $\text{C}_s$  on the surface. The Ni-Cu tubing reduces the number of places where  $\text{C}_s$  can be formed and held and decreases the extent of methanation of CO and  $\text{CO}_2$ .<sup>3</sup>

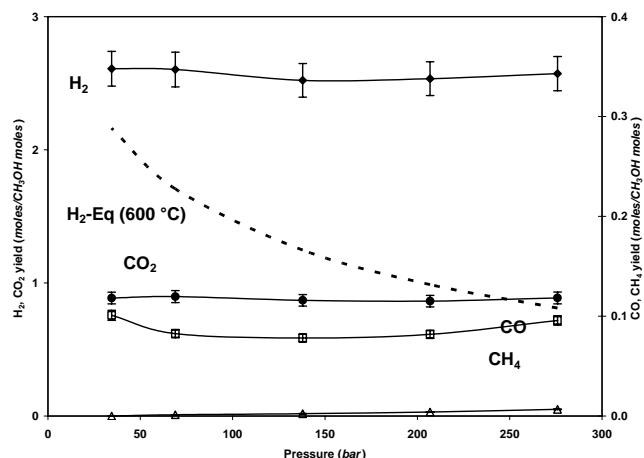


**Figure 4.** Effect of pressure on gas yield with Ni-Cu reactor. (10 wt.% methanol, 1 mL/min, 600 °C, reactor length = 1 m)

The performance of the Inconel 600 reactor can be improved by adding  $\text{K}_2\text{CO}_3$  or KOH in aqueous methanol. **Figure 5** shows the increase in the  $\text{H}_2$  yield and the decrease in the  $\text{CH}_4$  yield.

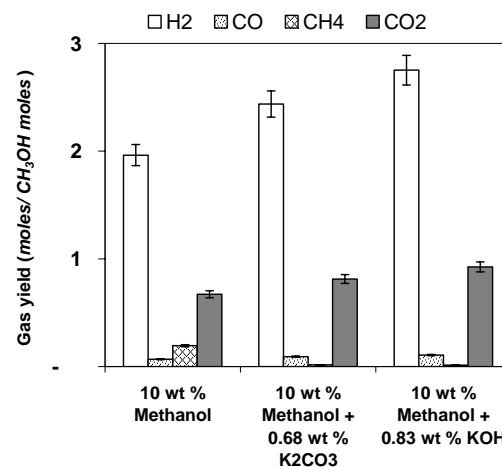


**Figure 5.** Effect of  $\text{K}_2\text{CO}_3$  and KOH addition. (10 wt.% methanol, 1 mL/min, 700 °C, reactor length = 2 m)

## Conclusions

$\text{CH}_4$  formation during reforming of methanol in supercritical water can be suppressed by (1) operating at a low residence time, (2) using Ni-Cu reactor or (3) adding  $\text{K}_2\text{CO}_3$  or KOH in the feed.

## References

- <sup>1</sup> Boukis, N.; Diem, V.; Habicht, W.; Dinjus, E. *Industrial & Engineering Chemistry Research* **2003**, 42(4), 728-735.
- <sup>2</sup> Antal, Michael Jerry, Jr.; Allen, Stephen Glen; Schulman, Deborah; Xu, Xiaodong; Divilio, Robert J. *Industrial & Engineering Chemistry Research* **2000**, 39(11), 4040-4053.
- <sup>3</sup> Araki, M.; Ponec, V. *Journal of Catalysis* **1976**, 44(3), 439-48.

# COPRODUCTION OF HYDROGEN AND CHEMICALS BY VAPOR PHASE DECOMPOSITION OF METHANOL

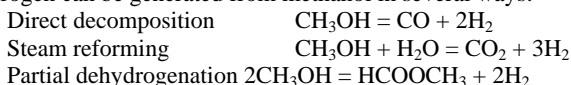
F. Shi, Y. Zhang, J. W. Tierney and I. Wender

Department of Chemical Engineering  
University of Pittsburgh, Pittsburgh, PA 15261, USA

## Introduction

Methanol is produced in huge amounts from synthesis gas derived chiefly from natural gas. In 2003 world capacity for methanol synthesis was over 50 million tons per year. Very large plants are being built near resources of cheap natural gas. Methanol is a hydrogen-rich liquid, and provides a great deal of convenience in storage, transport and handling as a source of hydrogen.

Hydrogen can be generated from methanol in several ways:



Partial dehydrogenation of methanol produces hydrogen as well as methyl formate (MF). MF has been proposed as a building block for a number of chemicals. It is a stable liquid and can be catalytically converted to a number of important chemicals including dimethyl formamide, formamide, ethylene glycol, acetic acid, dimethyl carbonate and formaldehyde.<sup>1-4</sup>

Since MF is an intermediate in a series of reactions, fast desorption and diffusion is essential for high selectivity to MF and hydrogen. In this study, works has started on the gas phase dehydrogenation of methanol to produce hydrogen and MF on a series of copper-based catalysts. The effects of supports and promoters are under investigation. The formation of hydrogen via steam reforming is also of interest.

## Experimental

**Catalyst preparation.** A series of copper-based catalysts were prepared by incipient wetness impregnation of aqueous  $\text{Cu}(\text{NO}_3)_2$  solution onto various supports: Zeolite (ZSM-5),  $\text{Al}_2\text{O}_3$ , and  $\text{MgO}$ . The impregnated samples were dried at  $110^\circ\text{C}$  for at least 8 h prior to calcining at  $350^\circ\text{C}$  in air for 3 hours. Before reaction, catalysts were reduced at  $250^\circ\text{C}$  with 50 ml/min  $\text{H}_2/\text{Ar}$  gases for 3 hours.

**Catalyst testing.** Methanol dehydrogenation experiments, including direct decomposition and steam reforming, were tested in a quartz micro reactor with 0.6-0.8 g copper catalyst loading. Liquid methanol is fed using a syringe pump (100DX, ISCO) at a rate of 3 ml/hr and then is evaporated and mixed with 20 ml/min Ar in a 100 ml evaporator at  $150^\circ\text{C}$ . All gas mixtures are heated with heating tapes before entering the micro-reactor and GC as well. Products were analyzed by two on-line Hewlett Packard GCs: one equipped with a TCD detector and with a Carbonsphere packed column (6 feet, 3/8 in) for analysis of  $\text{H}_2$ ,  $\text{CO}$ ,  $\text{CH}_4$ ,  $\text{CO}_2$ ; another equipped with a FID and HP-5 capillary column for analysis of methanol, methyl formate, dimethyl ether and other organic products. Liquid products are also collected with a cold trap at  $-80^\circ\text{C}$  and then are analyzed using GC-MS.

## Results and Discussions

**Thermodynamic calculations.** Thermodynamic calculations for methanol dehydrogenation, including direct decomposition and steam reforming (methanol/water=1), have been conducted using ASPEN Plus 12, based on Gibbs free energy minimization method. Results for hydrogen and MF production are shown in Figure 1. At temperatures below  $200^\circ\text{C}$ , methanol dehydrogenation to MF and hydrogen is favored; at temperatures above  $300^\circ\text{C}$ , complete

decomposition of methanol to  $\text{H}_2$  and  $\text{CO}$  dominates. Although steam reforming can produce more hydrogen than methanol dehydrogenation, it decreases the formation of MF greatly.

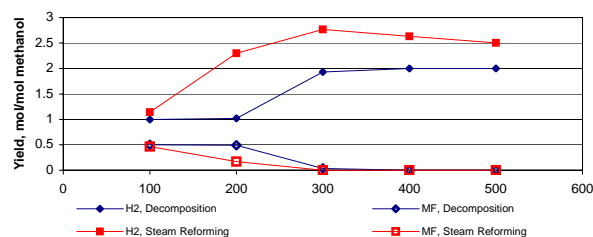


Figure 1.  $\text{H}_2$  and MF productions by methanol dehydrogenation

**Catalyst performance.** Methanol dehydrogenation experiments have been carried out on copper based catalysts at different temperatures, from  $150^\circ\text{C}$  to  $250^\circ\text{C}$  with  $10^\circ\text{C}$  intervals. Methanol conversion and hydrogen production at various temperatures are shown in Figures 2 and 3, respectively.

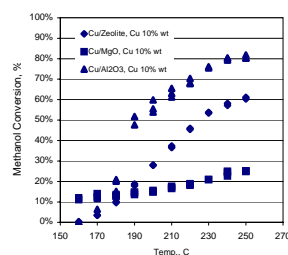


Figure 2. Methanol conversion at different temperatures

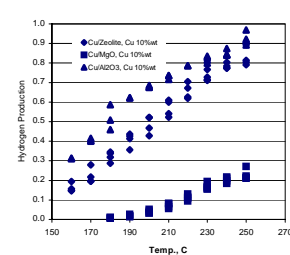


Figure 3. Hydrogen production at different temperatures

Figure 2 shows that the conversion of methanol increases with increase in temperature with three catalysts.  $\text{Cu}/\text{Al}_2\text{O}_3$  is the most active catalyst and the conversion of methanol can reach 80% at  $250^\circ\text{C}$ .  $\text{Cu}/\text{MgO}$  is the least active. Methanol conversion is below 25%. Hydrogen yields, shown in Figure 3, show the same trend with the conversion of methanol:  $\text{Cu}/\text{Al}_2\text{O}_3 > \text{Cu}/\text{ZSM-5} > \text{Cu}/\text{MgO}$ . Dimethyl ether is also formed on  $\text{Cu}/\text{ZSM-5}$  and  $\text{Cu}/\text{Al}_2\text{O}_3$  catalysts due to acidity of the supports. In the above experiments, only limited amounts of MF are obtained. Modifications of catalysts are under investigation to improve MF selectivity. Effect of water concentration on  $\text{H}_2$  and MF formation is also being studied.

## Summary

Thermodynamically, lower temperature favors MF formation and the presence of steam decreases MF selectivity. Cu-based catalysts are active for decomposition of methanol in the order of  $\text{Cu}/\text{Al}_2\text{O}_3 > \text{Cu}/\text{ZSM-5} > \text{Cu}/\text{MgO}$ . Promoters are needed to improve MF selectivity.

**Acknowledgment.** We thank the U.S. Department of Energy for financial support under grant No. DE FC26 99FT40540.

## References

1. Iwasa, N.; Takezawa, N. *Top. Catal.* **2003**, 22, 215.
2. Hashimoto, K.; Toukai, N. *J. Mol. Catal. A* **2002**, 186, 79.
3. Shreiber, E. H.; Roberts, G. W. *Appl. Catal. B* **2000**, 26, 119.
4. Lee, J. S.; Kim, J. C.; Kim, Y. T. *Appl. Catal.* **1990**, 57, 1.

# SBA-15 SUPPORTED COBALT AND IRON CATALYSTS FOR FISCHER-TROPSCH SYNTHESIS

Dae Jung Kim <sup>a</sup>, Brian C. Dunn <sup>a</sup>, Min Kang <sup>b</sup>,  
Jae Eui Yie <sup>c</sup>, and Edward M. Eyring <sup>\*cd</sup>

<sup>a</sup> Department of Chemistry, University of Utah Salt, Lake City,  
UT 84112, USA

<sup>b</sup> Department of Molecular Science & Technology, Ajou University,  
Suwon 442-749, South Korea

<sup>c</sup> Department of Applied Chemistry, Ajou University,  
Suwon 442-749, South Korea

## Introduction

Fischer-Tropsch (FT) synthesis is a promising pathway to very clean alternative fuels derived from coal syngas. It is important to develop active catalysts with high selectivity for production of long chain hydrocarbons. The activity of catalysts for FT synthesis depends primarily on the overall amount of exposed metal atoms. Thus, a highly active catalyst requires a high dispersion of cobalt metal. Mesoporous silica materials such as SBA-15 have been recently used as supports for cobalt.<sup>1-4</sup> The high surface area (500 - 1500 m<sup>2</sup>/g) of the mesoporous materials gives higher metal dispersions at higher cobalt loadings compared with conventional amorphous silicas. Furthermore, the uniform pore diameters (2 - 30 nm) of the mesoporous silica materials permit better control of the cobalt particle size and the distribution of hydrocarbon products from the FT synthesis.<sup>5</sup> We have proposed that surface modification of SBA-15 via silylation increases the catalytic activity and hydrocarbon selectivity in FT synthesis.<sup>6</sup>

The objectives of this present study are to determine the relative merits of impregnation methods, advantages of iron over cobalt and the consequences of aluminum incorporation in SBA-15 on catalytic activity in Fischer-Tropsch synthesis. Six different catalysts were prepared. The physical and chemical properties of the catalysts were obtained from N<sub>2</sub> adsorption/desorption, XRD and TPR experiments. The catalytic performance in FT synthesis was evaluated with a fixed-bed reactor.

## Experimental

**Catalyst preparation.** SBA-15 was obtained by a procedure described elsewhere.<sup>6,7</sup> Triblock polymer Pluronic P123 (EO<sub>20</sub>PO<sub>70</sub>EO<sub>20</sub>,  $M_{av}$  = 5800, BASF) was used as the structure-directing agent of SBA-15. Anhydrous sodium metasilicate (Na<sub>2</sub>SiO<sub>3</sub>, Aldrich) was used as the silica source of SBA-15. Aluminum incorporation in SBA-15 was achieved using the following post-synthesis procedure. 1.0 g of calcined pure SBA-15 was added to a 50 mL ethanol solution containing AlCl<sub>3</sub> (Aldrich). The mixture was stirred at ambient temperature overnight, and filtered using a glass membrane filter. The filtered sample was dried in air at 100 °C overnight, and then calcined in air at 550 °C overnight. The amount of incorporated aluminum was analyzed by ICP-AES.

SBA-15 supported cobalt catalysts were prepared by three different cobalt impregnation methods: incipient wetness, post-synthesis and supercritical solvent. The cobalt post-synthesis impregnation was similar to that used to graft aluminum on SBA-15. The impregnation of the SBA-15 with cobalt using a supercritical solvent proceeded as follows: The SBA-15 was added to a 250 mL ethanol solution of Co(NO<sub>3</sub>)<sub>2</sub>·6H<sub>2</sub>O, and stirred at ambient temperature for 1 h. The suspension was transferred to an autoclave placed inside a furnace. The autoclave was purged ten times with 200 psi N<sub>2</sub> to remove any oxygen trapped in the system. The autoclave

was heated to 350 °C at 5 °C/min, then held at 350 °C for 3 h. The pressure inside the autoclave was maintained at 2000 psi by controlled venting through a high-pressure valve. The system was cooled to 200 °C, and the gas inside the autoclave was vented for 1 h. The system was then cooled to ambient temperature. The cobalt impregnated sample was calcined in air at 550 °C overnight. In this study, iron impregnated SBA-15 samples were prepared by incipient wetness impregnation using Fe(NO<sub>3</sub>)<sub>3</sub>·9H<sub>2</sub>O dissolved in ethanol solution. All calcined samples were reduced under hydrogen at 500 °C for 10 h to obtain active metallic cobalt or iron for the FT synthesis. Specifications of SBA-15 supported cobalt and iron catalysts used in this study are shown in Table 1.

**Table 1.** Specification of SBA-15 supported cobalt and iron catalysts.

Catalyst	Silica	Precursor	Co loading (Wt %)	Loading method
CAT1	SBA15	Co(NO <sub>3</sub> ) <sub>2</sub>	6	IW
CAT2	SBA-15	Co(ac) <sub>2</sub> <sup>b</sup>	6	PS
CAT3	SBA-15	Co(NO <sub>3</sub> ) <sub>2</sub>	6	SS
CAT4	SBA-15	Co(NO <sub>3</sub> ) <sub>2</sub>	20	IW
CAT5	SBA-15	Fe(NO <sub>3</sub> ) <sub>3</sub>	20	IW
CAT6	AlSBA-15	Fe(NO <sub>3</sub> ) <sub>3</sub>	20	IW

<sup>a</sup> IW: incipient wetness, PS: post synthesis, SS: supercritical solvent impregnation

<sup>b</sup> Co(ac)<sub>2</sub> is anhydrous cobalt acetate

**Catalyst characterization.** To evaluate the pore structure of the catalyst samples, nitrogen adsorption isotherms were measured using an Autosorb-1 instrument (Quantachrom). The isotherms were used to calculate the BET specific surface area ( $S$ ), total pore volume ( $V_t$ ), and average pore diameter ( $D_p$ ). The pore structure of the samples was also evaluated using XRD patterns. The reduction of cobalt oxides in the sample was evaluated by temperature programmed reduction (TPR, Micromeritics). The H<sub>2</sub> consumption of the sample was calculated using the reduction of CuO as the standard.

**FT synthesis and product analysis.** The FT synthesis was carried out in a fixed-bed stainless steel reactor (5 mm I.D. and 168 mm length) at 100 psi and 265 °C. An H<sub>2</sub>/CO molar ratio of 2 was used, and a ratio of sample weight to total gas flow rate (W/F) was 0.47 - 0.91. The gas flow rates for reactant gases (CO, H<sub>2</sub>) and internal standard (Ar) were controlled by mass flow controllers (MKS). Iron carbonyl impurities in the CO reactant stream were removed by a PbO<sub>2</sub>/Al<sub>2</sub>O<sub>3</sub> trap. The test for the FT synthesis was carried out for 36 h on stream. Reactants and hydrocarbon products were analyzed by gas chromatography (Shimadzu). The GC oven was heated using a heating program as follows: 10 °C for 4 min, then heating from 10 to 350 °C with the heating rate of 20 °C/min and holding at 350 °C for 10 min. Reactants were separated on a capillary column (CarboPlot, 0.53 mm I.D. and 30 m length) with a TCD detector. Hydrocarbon products were separated on a capillary column (DB-5, 0.25 mm I.D. and 10 m length) with an FID detector.

## Results and Discussion

The results of XRD patterns and nitrogen adsorption/desorption isotherms revealed that all cobalt catalysts having 6 wt% cobalt had the 2-D hexagonal structure of pure SBA-15. Pore structural parameters calculated from nitrogen adsorption/desorption isotherms for the cobalt SBA-15 catalysts are listed in Table 2. The BET surface area, pore volume and pore diameter of SBA-15 are decreased by cobalt impregnation. However, the three cobalt catalysts prepared by three different impregnation methods have similar pore structural values. This implies that the impregnation method does not have a significant impact on the pore structure of SBA-15.

**Table 2.** Physical and chemical properties of SBA-15 supported cobalt catalysts.

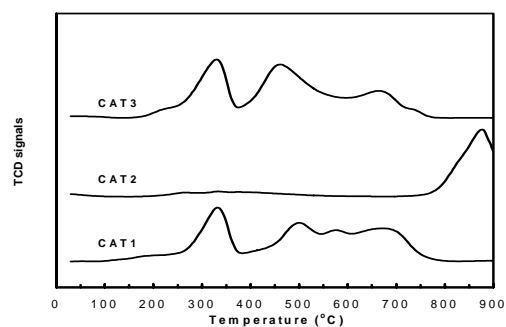
Catalyst	S <sup>a</sup> (m <sup>2</sup> /g)	V <sub>t</sub> <sup>b</sup> (cc/g)	D <sub>p</sub> <sup>c</sup> (nm)	Co <sub>3</sub> O <sub>4</sub> <sup>d</sup> Diameter (nm)	Reduction <sup>e</sup> (%)
Pure SBA-15	724	1.243	8.09	-	-
1CAT	465	0.811	8.08	11.1	49
2CAT	472	0.858	8.08	-	18
3CAT	461	0.815	8.08	11.6	63

<sup>a</sup> BET Surface area, <sup>b</sup> Total pore volume, <sup>c</sup> average pore diameter,

<sup>d</sup> Co<sub>3</sub>O<sub>4</sub> crystallite diameter calculated from the widths of XRD peaks using the Scherrer equation (2 theta = 36.68°),

<sup>e</sup> reduction degree of cobalt oxides during TPR at 30 – 500 °C.

The mean Co<sub>3</sub>O<sub>4</sub> crystallite sizes deduced from the XRD data using the Scherrer equation and the reduction percentage of the cobalt oxides at temperatures less than 500 °C are presented in Table 2. The XRD peak at 36.68° for CAT2 was not detected. This suggests that most of cobalt oxides are present as cobalt silicates in the framework of the SBA-15, and the average crystallite size of Co<sub>3</sub>O<sub>4</sub> on the surface of the SBA-15 is very small. The mean Co<sub>3</sub>O<sub>4</sub> crystallite size on CAT3 is slightly larger than on CAT1. This result indicates that the crystallite size of Co<sub>3</sub>O<sub>4</sub> is clearly dependent on the impregnation method. Figure 1 shows TPR profiles of three cobalt catalysts, CAT1, CAT2 and CAT3. CAT1 and CAT3 show similar TPR profiles with three typical peaks. However, the TPR profile of CAT2 with two peaks is significantly different.

**Figure 1.** TPR profiles of three cobalt catalysts

For CAT1 and CAT3, the first peak at temperatures less than 380 °C can be assigned to the reduction of Co<sub>3</sub>O<sub>4</sub>, and the second peak in the 380 - 600 °C range corresponds to the reduction of cobalt oxides strongly interacting with the SBA-15. The third peak in the 600 - 760 °C range can be attributed to the reduction of cobalt oxides very strongly interacting with the SBA-15. The maximum temperatures of the three peaks for CAT3 are located at lower temperatures than for CAT1. In particular, the intensity of the third peak for CAT3 is very low. This suggests that highly irreducible cobalt oxides on CAT3 are less prevalent than on CAT1. CAT2 shows two peaks in its TPR profile. The first peak is at temperatures in the range of 200 – 500 °C, and the second peak is located at temperatures above 760 °C, corresponding to the reduction of cobalt oxides in the framework of SBA-15.

The reduction percentage of the cobalt oxides at temperatures less than 500 °C are presented in Table 2. CAT3 shows the highest reducibility of cobalt oxides among the three catalysts prepared by different impregnation methods. According to the TPR results, undesirable cobalt oxides (those not easily converted to active cobalt metal at lower temperature) were abundantly produced in CAT1.

Catalytic activities of SBA-15 supported cobalt and iron catalysts in FT synthesis are summarized in Table 3.

**Table 3.** CO conversion, hydrocarbon selectivity and chain growth probability of SBA-15 supported cobalt and iron catalysts

Catalyst	W/F (g h/mol)	CO conversion (%)	Product selectivity (C mol%) <sup>a</sup>				
			C <sub>1</sub>	C <sub>2</sub> -C <sub>4</sub>	C <sub>5</sub> -C <sub>10</sub>	C <sub>10</sub> +	
CAT1	0.73	15.7	8.6	38.6	39.0	13.8	0.86
CAT2	0.91	4.6	15.8	56.8	24.2	3.2	0.82
CAT3	0.67	21.1	7.3	32.4	45.3	15.0	0.88
CAT4	0.55	22.2	7.2	32.3	46.5	14.0	0.88
CAT5	0.47	23.8	6.2	6.5	32.8	54.5	0.95
CAT6	0.47	32.5	4.9	6.1	27.3	61.7	0.98

<sup>a</sup> chain growth probability obtained from Anderson-Schulz-Flory equation

CO conversion and higher hydrocarbon selectivity can be related to the reducibility of the cobalt oxides and pore structure of a cobalt catalyst. The three samples (CAT1, CAT2, CAT3) having the same loading of cobalt showed similar values in BET surface area, pore volume and average pore size. However, the three samples showed differences in the reducibility of cobalt oxides. CAT3 shows the highest CO conversion, C<sub>5</sub> selectivity and chain growth probability among the three catalysts obtained by three different cobalt impregnation methods. This result is quite consistent with the TPR result. In this study, to investigate the effect of active metal and aluminum incorporation of SBA-15 on catalytic activity, we prepared a cobalt catalyst (CAT4) and two iron catalysts (CAT5, CAT6). The three samples have the same metal loading. CAT5 shows higher CO conversion, C<sub>5</sub> selectivity and chain growth probability than CAT4. This indicates that iron in the SBA-15 is more effective than cobalt for FT synthesis. As the results of TPR and EXAFS tests, after aluminum incorporation of SBA-15, reducible iron oxides such as Fe<sub>2</sub>O<sub>3</sub> on CAT6 were greatly increased compared to CAT5. This indicates that the increase of reducible iron oxides leads to an increase in catalytic activity of the iron catalyst.

In a summary, the cobalt impregnation method has a significant effect on catalytic activity and selectivity through differences in reducibility of cobalt oxides. Aluminum added iron-based catalyst is also advantageous.

## Acknowledgment

The U.S. Department of Energy provided financial support to the Consortium for Fossil Fuel Science for this study (contract # DE-FC26-02NT41954).

## References

- Girardon, J. S.; Lermontov, A. S.; Gengembre, L.; Chernavskii, P. A.; Griboval-Constant, A.; Khodakov, A. Y. *J. Catal.* **2005**, *230*, 339-352.
- Okabe, K.; Wei, M.; Arakawa, H. *Energy & Fuels* **2003**, *17*, 822-828.
- Martinez, A.; Lopez, C.; Marquez, F.; Diaz, I. *J. Catal.* **2003**, *220*, 486-499.
- Panpranot, J.; Goodwin, J. G.; Sayari, A. *Catal. Today* **2002**, *77*, 269-284.
- Wang, Y.; Noguchi, M.; Takahashi, Y.; Ohtsuka, Y. *Catal. Today* **2001**, *68*, 3-9.
- Kim, D. J.; Dunn, B. C.; Cole, P.; Turpin, G.; Ernst, R. D.; Pugmire, R. J.; Kang, M.; Kim, J. M.; Eyring, E. M. *Chem. Commun.* **2005**, 1462-1464.
- Kim, J. M.; Stucky, G. D. *Chem. Commun.* **2000**, 1159-1160.

# EFFECT OF PROCESS PARAMETERS ON LIGHT OLEFINS PRODUCTION FROM METHANOL AND SYNGAS OVER SAPO CATALYSTS

Luckner Jean<sup>a</sup>, Xiwen Huang<sup>a</sup> and James A. Guin<sup>a</sup>  
Gregory C. Turpin<sup>b</sup> and Richard D. Ernst<sup>b</sup>

<sup>a</sup>Department of Chemical Engineering  
Auburn University, Auburn, AL, 36849-5127

<sup>b</sup>Department of Chemistry  
University of Utah, Salt Lake City, UT, 84112-0850

## Introduction

The recent spike in energy prices has renewed attention on the production of chemicals from sources other than petroleum and focused attention on fossil fuels which are currently not recovered. In this light the use of SAPO catalysts in converting syngas either directly or indirectly to chemicals e. g. C<sub>2</sub>-C<sub>4</sub> olefins, is of interest. The main feedstock of current interest is remote or flared natural gas, although any feedstock convertible to syngas is technically viable. This means that coal and biomass are potential resources for chemicals currently produced from petroleum. We are especially interested in C<sub>2</sub>-C<sub>4</sub> olefins.

Flanigan, et al. have presented many of the most important properties of the SAPO catalysts in their foundational work<sup>1</sup>. A good review of the chemistry of methanol to hydrocarbons is presented by Stocker<sup>2</sup>. In his review it is noted that the pathway for methanol to olefins (MTO) is via a consecutive reaction with the dimethyl ether (DME) intermediate.

Many parameters such as acidity, pore size, composition, and method of preparation influence the activity of SAPO catalysts. Thus a particular SAPO, e. g., SAPO-34, may behave differently depending on its history and manner of preparation. A main obstacle in the MTO process is the rapid deactivation of the catalysts due to coke formation; however, regeneration is possible by oxidation as in a recirculating fluid bed. Here we have studied the effect of particle size on the activity, selectivity and lifetime of several small pore SAPO catalysts in the MTO reaction. Particle size variation was accomplished by grinding. It is possible that grinding could induce changes in the crystalline structure of the catalysts, however, this was not determined in our study, the main focus being on the particle size variations and the resulting reaction effects. A few other studies have examined the effects of particle size on this reaction<sup>3,4</sup>. We also report preliminary results on the effect of Ru incorporation on SAPO performance.

## Experimental

The original SAPO catalysts used in our present work were samples prepared previously in our laboratory by Adekkanattu<sup>5-8</sup>. Studies were performed on SAPO-34, 44, 47, and 56. Original samples were ground in a Wig-L-Bug (Dentsply/Rinn) grinder with agate vial and ball for various times. Particle size was examined by SEM before and after grinding.

MTO reactions were performed at 1 atm in a quartz tube fixed bed, generally at 400 °C, using 0.3 g catalyst and 0.003 ml/min liquid methanol vaporized into nitrogen at 36 ml/min. (WHSV = 0.5 hr<sup>-1</sup>). In addition to particle size, effects of temperature and incorporation of Ru were also studied<sup>9</sup>. Products were analyzed by GC with FID and Plot-Q capillary column. More details are provided in the thesis by Jean<sup>10</sup>.

## Results and Discussion

**Figure 1** shows SEM micrographs of (a) the original SAPO-44 particles and (b) after grinding for 15 min. The reduction in particle size is fairly obvious from the scales on the figures, although some of the finer particles tend to form agglomerates. **Figures 2** (a) and (b) show the product distribution from MTO reactions over these SAPO-44 particles. We see that the ground particles have longer lifetimes, having increased from ca. 4 hrs to 10 hrs for the production of C<sub>2</sub>-C<sub>4</sub> olefins. The selectivity of ethylene to propylene is not appreciably altered by the size reduction, however a notable change in selectivity to DME is apparent, as a result of the grinding. This latter finding is in keeping with the product distribution expected from particle size reduction in a diffusion controlled reaction with DME intermediate, i. e., an increase in selectivity of the intermediate due to lower intraparticle diffusional resistance<sup>11</sup>. As shown in **Figure 3**, similar results were obtained at 5 and 10 min grinding times, although particle sizes at lesser grinding times as viewed by SEM were not dramatically different from **Figure 1**(b). Similar changes in catalyst lifetime and DME selectivity, though not as large, were found in the performance of SAPO-34, 47, and 56. In a few cases, the grinding process caused a decrease in activity. An attempt to restore the activity of a spent SAPO-56 sample was unsuccessful, perhaps indicating the deactivation process, e. g., coke deposition, was uniformly spread throughout the particles, as opposed to being preferentially located around the external surface.

**Figure 4** shows the performance of Ru-SAPO-44. Comparison with the unmodified catalyst in **Figure 2**(a) shows a small improvement, ca. 1 hr, in C<sub>2</sub>-C<sub>4</sub> olefins based lifetime. Ru-SAPO-56 was also slightly improved, while, SAPO-34 was not improved by the Ru addition. These results are interesting, however, more work would be required, perhaps with other metals and conditions to fully determine the benefits of metals addition to the SAPOs.

## Conclusions

Particle size reduction shows potential as an effective way to increase lifetime of SAPO catalysts based on C<sub>2</sub>-C<sub>4</sub> olefins production, although for a completely deactivated catalyst grinding alone will not regenerate the catalyst. The selectivity of the intermediate DME is increased by particle size reduction in keeping with diffusional effects on selectivity of an intermediate in a series reaction pathway. Ru addition had only a small effect on the SAPO lifetimes in this limited study.

**Acknowledgment.** This research was supported by the U.S. Department of Energy Office of Fossil Energy, National Energy Technology Laboratory (NETL), under DOE Contract DE-FC26-02NT41594. The authors wish to acknowledge Dr. P. M. Adekkanattu for preparing the original SAPO catalysts.

## References

1. Flanigan, E. M., Lok, B. M., Patton, R. L. and Wilson, S. T.: *Proc. 7<sup>th</sup>. Int. Zeolite Conf.*, Tokyo, 103, **1986**.
2. Stocker, M., *Microporous and Mesoporous Materials* 29, **1999**, 3 – 48.
3. Chen, D., Kjell, M. Fuglerud, T., Holmen, A., *ibid.*, 191.
4. Dahl, I. M. Wendelbo, R., Andersen, A., Akporiaye, D. Mostad, H. Fuglerud, T., *ibid.*, 159.
5. Annual Report for Period May 2001- May 2002, DOE Cooperative Agreement No. DE-FC26-99FT40540, Prepared by Consortium for Fossil

- Fuel Science, University of Kentucky.
6. Annual Report for Period May 2002- May 2003, DOE Cooperative Agreement No. DE-FC26-02NT41594, Prepared by Consortium for Fossil Fuel Science, University of Kentucky.
  7. Obrzut, D.L., Adekkanattu, P. M., Thundimadathil, J., Liu, J., Dubois, D.R., Guin, J.A., *React. Kin. Catal. Lett.*, 80(1) **2003** 113.
  8. Dubois, D.R., Obrzut, D.L., Liu, J. Thundimadathil, J., Adekkanattu, P. M., Guin, J. A. , Punnose, A. Seehra, M. S., *Fuel Proc. Technol.*, 83(1-3), **2003**, 203.
  9. Wilson, D.R., Stahl, L., Ernst, R. D., *Organometallic Synthesis*, 3, **1986**, 136.
  10. Jean, L., M. S. Thesis, Auburn University, **2005**.
  11. Petersen, E. E., *Chemical Reaction Analysis*, Prentice Hall, **1965**, p. 97.

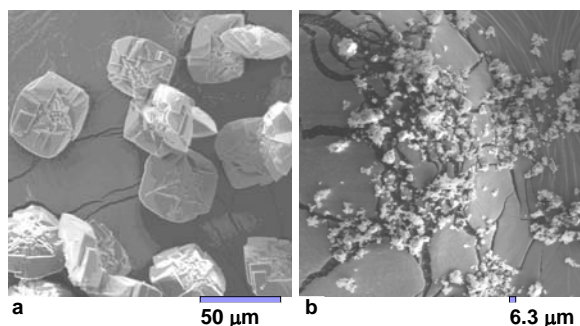


Figure 1. (a) SAPO-44 (Original Particles)  
(b) SAPO-44 (After 15 min Grinding)

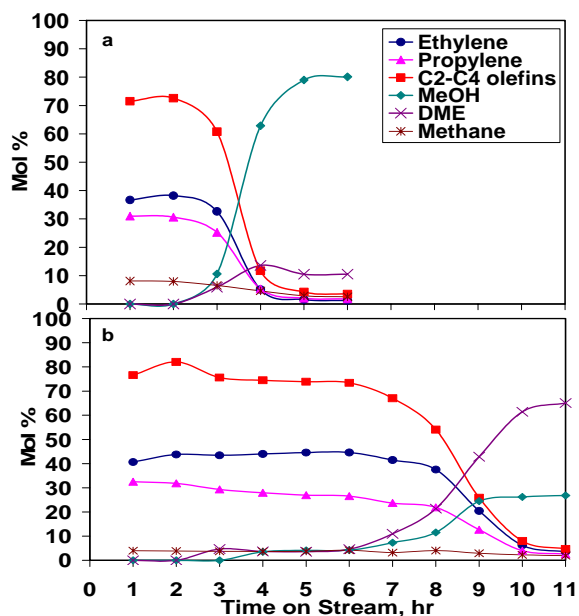


Figure 2. Product Distribution over: (a) Original Particles; (b) Ground Particles.

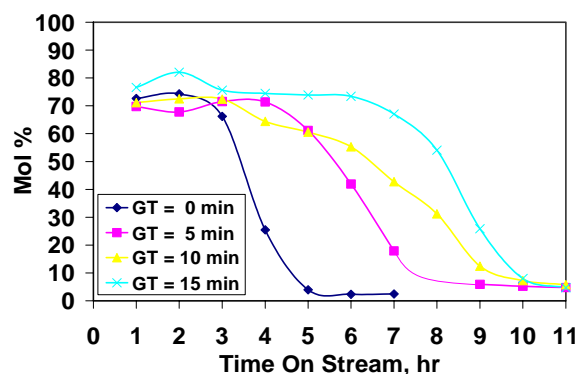


Figure 3. Effect of Grinding Time (GT) on C<sub>2</sub> - C<sub>4</sub> Olefins Production over SAPO-44.

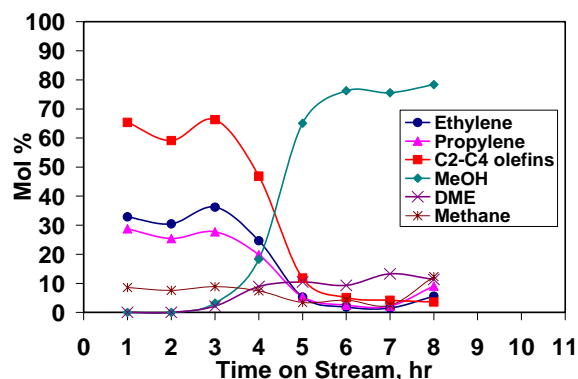


Figure 4. Product Distribution over Ru-SAPO-44.

# CATALYTIC METHANE DECOMPOSITION USING A FLUIDIZED BED REACTOR FOR HYDROGEN PRODUCTION

Shankang Ma, Yuguo Wang, Naresh Shah, Gerald P. Huffman

University of Kentucky, 533 S. Limestone Street, Suite 107,  
Lexington, KY 40508-4005

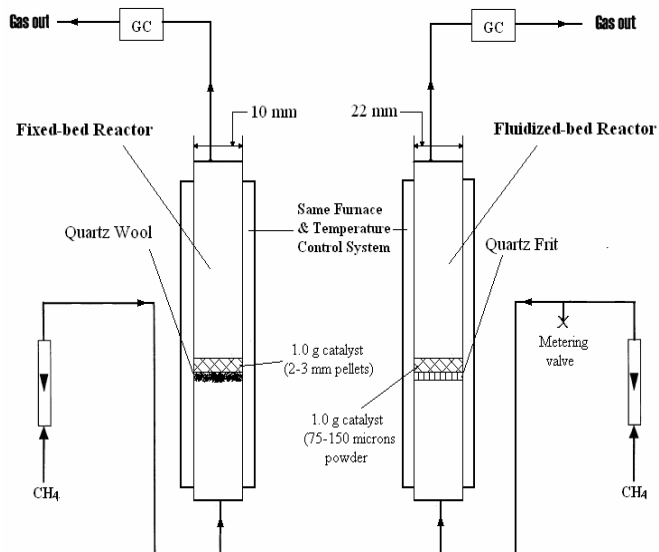
## Introduction

Previously, we have developed alumina supported binary catalysts, (M-Fe)/Al<sub>2</sub>O<sub>3</sub> (M=Pd, Mo, or Ni), that are very active for catalytic dehydrogenation of lower alkanes to produce pure hydrogen and carbon nanotubes.<sup>1,2,3</sup> One major setback in such laboratory scale experiments is accumulation of carbon nanotubes (CNT), a potentially valuable byproduct, within the reactor. In a fixed bed mode of operation, this fouling due to CNT tangling and accumulation and quickly starts hindering the flow of the reactant and product gas streams, builds back pressure and reduces activity.

One possible way to dislodge nanotubes anchored to the catalyst particles on the surface of the alumina support is to mechanically breaking the nanotubes at these linkages by physical agitation. Fluidization of the bed should induce turbulent flow of the catalytic bed media and repeated inter-particle collisions that could shear nanotubes from the active metallic catalysts. Once freed, fine nanotubes should be carried away by the fluidizing gas stream to be externally collected and the catalyst should continue to further decompose methane, producing additional hydrogen and carbon nanotubes. In this paper, we report results from the preliminary tests carried out to validate the aforementioned hypothesis.

Most of the hydrogen production work using fluidized bed reported in the literature concern with the production of syngas.<sup>4,5,6,7</sup> When used for the production of carbon nanotubes, fluidized bed reactors are typically fed with higher carbon content gases and not methane.<sup>8,9,10,11,12</sup> Lee et al.<sup>13</sup> have used a fluidized bed reactor for hydrogen production from catalytic decomposition of methane using activated carbon catalysts with very low methane conversion. Weizhong et al.<sup>14</sup> have employed a two-stage fluidized bed reactor for production of hydrogen and carbon nanotubes from methane.

## Experimental



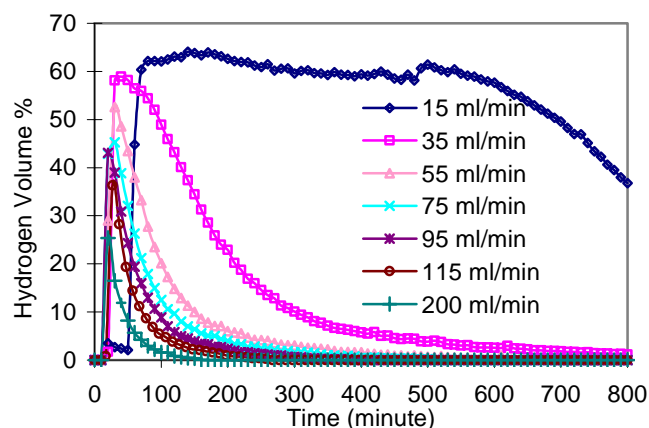
**Figure 1.** Schematics comparing fixed-bed (old) reactor and fluidized-bed (new) reactor

Figure 1 is a schematic diagram comparing salient features of our old fixed bed reactor with the new fluidized bed reactor. The two setups are identical except for larger reactor diameter (for high methane flow rate required for fluidization) and a quartz frit fused to the quartz wall of the reactor instead of a quartz wool plug (for catalyst support). Because there is no thermal methane decomposition at a reactor temperature of 700 °C, the pores in the quartz frit were never plugged with carbon. By increasing the methane flow rate from 10 ml/min to >100 ml/min, the reactor mode can be varied from fixed bed to fluidized bed. At high methane flow rate (15 l/min), the entire reactor can be emptied of the catalyst and attached CNT very quickly and new catalyst can be added to the reactor from the top (not shown in the schematic) at low or zero methane flow rate.

For all fluidized bed reactor experiments, 1 gram of as prepared 0.5%Mo-4.5%Fe/Al<sub>2</sub>O<sub>3</sub> catalyst was used at the reactor temperature of 650-700 °C. To achieve good fluidization, the catalyst fluidized bed particle size was kept between 70 and 150 microns.

## Results

Figure 2 shows volume percent hydrogen in the reactor exit stream as a function of time on stream for different methane feed flow rates. With increasing methane flow rate, hydrogen production efficiency decreases as methane-catalyst contact time decreases.



**Figure 2.** Time-on-stream hydrogen production at different methane flow rates.

**Table 1. Hydrogen production efficiency at different methane flow rates and different reactor modes**

	Methane Flow Rate (ml/min)	Linear Velocity (m/s)	Total Methane Input (ml) in 800 minutes	Total Hydrogen Produced (ml) in 800 minutes	Efficiency (H <sub>2</sub> /CH <sub>4</sub> )
Fixed Bed Mode	15	2.37	12000	9210	77%
	35	5.52	28000	4830	17%
	55	8.68	44000	3350	8%
	75	11.84	60000	3110	5%
Fluidized Bed Mode	95	14.99	76000	2830	4%
	115	18.15	92000	2000	2%
	200	31.57	160000	1790	1%

To compare efficiency of the hydrogen production, we have to compare areas under individual curves in figure 2. As shown in table 1, the reactor is most efficient in producing hydrogen at the lowest flow rate and highest reactant-catalyst contact time. As the flow rate increases, some of the methane just passes through the voids in the catalyst bed without coming in contact with any active metallic catalyst sites. At even higher flow rates, most of the methane acts simply as a fluidizing medium and not a reactant. As mentioned earlier, methane decomposition under these reaction conditions is purely a catalytic reaction and if a methane molecule does not come in direct contact with an active catalytic site, it will not undergo decomposition.

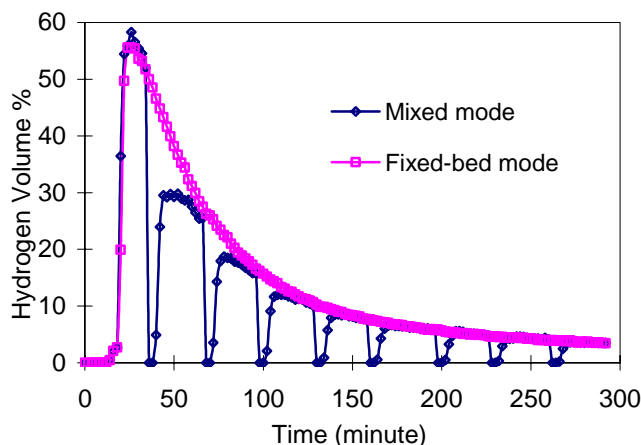


**Figure 3.** Comparison of fixed bed mode and mixed mode hydrogen production by catalytic methane dehydrogenation.

Based purely on these observations, there is no real advantage of operating the reactor in the fluidized mode. However, it is worth reflecting that the main reason for operating the reactor was not improving the activity. Rather, the tumbling and collisions of bed particles in a fluidized bed was hypothesized to cause separation of nanotubes from the anchoring metal catalyst sites. To achieve both high hydrogen production efficiency and separation of nanotubes, a periodic mode switching experiment was performed. In such an operation, the reactor will be mostly operated in the high efficiency, low flow rate, fixed bed mode for generation of hydrogen. At regular intervals, the flow rate can be increased for short durations, at the penalty of low hydrogen production efficiency, to fluidize the bed to separate nanotubes from the bed material and remove them from the reactor. Figure 3 compares hydrogen production for a fixed bed mode operation and a periodically fluidized fixed bed (mixed mode) mode of operation. It is evident that after short fluidization, the active catalyst sites do not regain their catalytic activity because of separation and harvesting of the nanotubes.

During initial shakedown experiments of the new reactor set-up at different methane flow rates, we had noticed that at the very high methane flow rate (15 l/min), the catalyst bed can be fluidized very vigorously and expanded completely out of the length of the tube. As a result, all the catalyst bed material can be ejected out of the reactor almost instantaneously at the operating temperature just by increasing the flow rate. Figure 4 shows the hydrogen production for four such replenishing/complete blow out cycles.

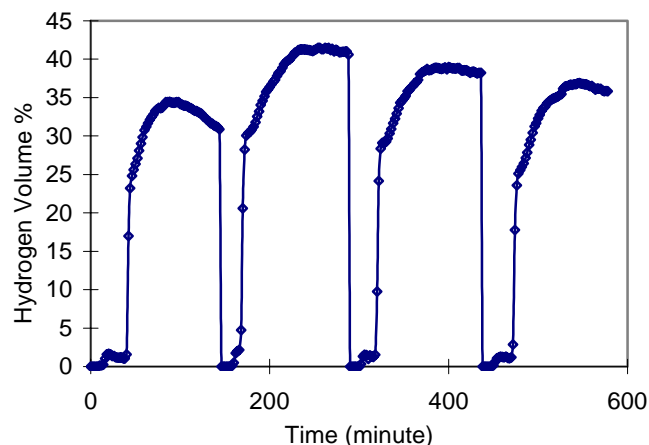


**Figure 4.** Semi-continuous hydrogen production by cyclic blowing out the catalyst bed with attached nanotubes and replenishing the reactor with completely new catalytic bed material at 650 °C.

### Conclusions

To overcome the fouling of the fixed bed reactor by carbon nanotubes in methane dehydrogenation and to make hydrogen and nanotubes production continuous, fluidized bed mode and mixed mode catalytic dehydrogenation experiments were performed. These experiments showed that the hydrogen production is most efficient only in a fixed bed mode at the lowest methane flow rate. The results also negated the validity of the hypothesis that the tumbling and inter particle collisions of bed material would efficiently separate nanotubes anchored to the catalyst bed particles. A very high methane flow rate was successfully used to rapidly blow the entire bed material and attached nanotubes out of the reactor. The reactor was then replenished with fresh catalyst at the operating temperature to generate hydrogen in a semi-continuous way.

**Acknowledgement.** This research was supported by the U.S. Department of Energy, Office of Fossil Energy, under the management of the National Energy Technology Laboratory, U.S. DOE Contract No. DE-FC26-02NT41594.

### References

- Shah, N.; Panjala D.; Huffman, G.P. *Energy & Fuels*, **2001**, 15(6), 1528.
- Shah, N.; Wang, Y.; Panjala D.; Huffman, G.P. *Energy & Fuels*, **2004**, 18(3), 727-735.
- Wang, Y.; Shah, N.; Huffman, G.P. *Catalysis Today*, **2005**, 99, 359-364.
- Santos, A.; Menendez, M. Monzon, A.; Santamaria, J.; Miro, E.E.; Lombardo, E.A. *J. Catal.* **1996**, 156, 83.
- Bharadwaj, S.S.; Schmidt, L.D. *J. Catal.* **1994**, 146, 11.
- Opoku-Gyamfi, K.; Adesina, A.A. *Appl. Catal. A: Gen.* **1999**, 180, 113.
- Tomishige, K., *Catalysis Today* **2004**, 89, 405-418.
- Wang, Y.; Wei, F.; Luo, G.; Yu, H.; Gu, G., *Chemical Physics Letters* **2002**, 364, 568-572.
- Qian, W.; Wei, F.; Wang, Z. *AIChE Journal* **2003**, 49(3), 619-625.
- Mauron, P.; Emmenegger, C.; Sudan, P.; Wenger, P.; Rentsch, S.; Züttel, A. *Diamond and Related Materials*, **2003**, 12, 780-785.
- Corrias, M.; Caussat, B.; Ayrat, A.; Durand, J.; Kihn, Y.; Kalck, P.; Serp, P. *Chem. Engr. Sc.*, **2003**, 58, 4475-4482.
- Venegoni, D.; Serp, P.; Feurer, R.; Kihn, Y.; Vahlas, C.; Kalck, P. *Carbon*, **2002**, 40, 1799-1807.
- Lee, K.K.; Han, G.H.; Yoon, K.J.; Lee, B.K. *Catalysis Today* **2004**, 93-95, 81-86.
- Weizhong, Q.; Tang, L.; Zhanwen, W.; Fei, W.; Zhifei, L.; Guohua, L.; Yongdan, L. *Appl. Catal. A: General*, **2004**, 260, 223-228.

# DETERMINATION OF DIFFERENT ELECTRONIC STATES OF COBALT IN FISCHER-TROPSCH CATALYSTS

M. S. Seehra, P. Dutta, and A. Manivannan

Physics Department  
West Virginia University  
Morgantown, WV 26506

## Introduction

Recently, a number of studies of Fischer-Tropsch (FT) synthesis using cobalt catalyst supported on high surface area xerogel [1], aerogel [2,3], SiO<sub>2</sub> and Al<sub>2</sub>O<sub>3</sub> [4,5] have been reported. The factors that effect the yields and product distribution of the FT products include operating temperature and pressure, surface area and pore size of the support, particle size and dispersion of cobalt and its electronic state (Co<sup>0</sup>, Co<sup>2+</sup>, Co<sup>3+</sup>). To prepare the Co loaded catalyst, Co is usually impregnated as an oxide, followed by reduction and/or calcination to produce the desired Co<sup>0</sup> state which is the active catalyst. In order to compare the yield and product distribution with Co loading, it then becomes essential to determine the concentration of the various electronic states and phases of Co present in the catalyst. In this work, we summarize the results of our recent investigations for determining the different oxidation states of Co and their concentrations in Co/xerogel, Co/aerogel, Co/SiO<sub>2</sub> and Co/Al<sub>2</sub>O<sub>3</sub> catalysts. Only summary of these results is presented below, with the details given in the quoted papers [1-5].

## Experimental

The crystalline phases present in a catalyst were determined by room temperature x-ray diffraction (XRD) in a Rigaku diffractometer using CuK<sub>α</sub> radiation ( $\lambda = 0.15418$  nm). The XRD technique is able to detect phases with concentration  $\geq 3\%$ . The magnetic phases such as Co<sup>2+</sup>, Co<sup>3+</sup>, Co<sup>0</sup>, CoO and Co<sub>3</sub>O<sub>4</sub> were determined by magnetic measurements which were done using a commercial SQUID (superconducting quantum interference device) magnetometer. Additional information on states such as Co<sup>2+</sup> was also determined by EMR (electron magnetic resonance) spectroscopy at the X-band frequency  $f = 9.28$  GHz with a variable temperature (4 K to 300 K) cryostat. The important information on the electron state is contained in the g-value given by the EMR resonance condition  $hf = g\mu_B H_0$ , where  $h$  is the Planck's constant,  $\mu_B$  is the Bohr magneton and  $H_0$  is the resonance field of the EMR lines.

## Results and Discussion

An example of the information obtained from the XRD studies is given in Fig. 1. Here we have shown the XRD patterns of Co/xerogel catalyst in which clear identification of Co<sup>0</sup>, CoO and the support SiO<sub>2</sub> (xerogel) is made. (This figure is from the supporting materials of Ref. 1). In the Co/SiO<sub>2</sub> catalysts of Ref. 4, the XRD studies could only detect Co<sub>3</sub>O<sub>4</sub>, and Co<sup>0</sup> and CoO were absent [4]. Thus which phases of Cobalt (Co<sup>0</sup>, CoO or Co<sub>3</sub>O<sub>4</sub>) are present in a catalyst depend on the experimental conditions the catalyst is exposed to and these different states can usually be detected by XRD.

Careful analysis of the temperature (T) and magnetic field (H) variation of the magnetization (M) provide additional details about the electronic states of cobalt and their concentrations. The presence of CoO and Co<sub>3</sub>O<sub>4</sub> are detected from the peaks in susceptibility  $\chi = M/H$  at temperatures  $T \approx 300$  K and  $T \approx 40$  K respectively [3-5] whereas if Co<sup>0</sup> is present, it dominates the measured magnetization from which its concentration can be determined [3]. In Fig. 2, we

show our recent data from Ref. 3 on the  $\chi$  vs. T variation in 10% Co/aerogel catalyst. The peak in  $\chi$  near 20 K is due to Co<sup>0</sup> nanoneedles with diameter  $d \approx 1$  nm, whereas the peak in  $\chi$  near 300 K (Fig. 3) is due to the presence of CoO. From the magnitude of the saturation magnetization of this sample at 5 K, the concentration of Co<sup>0</sup> was determined to be around 8%. If Co<sup>0</sup> is simultaneously present with either CoO or Co<sub>3</sub>O<sub>4</sub>, then from the behavior of the hysteresis loop of Co<sup>0</sup> in a field cooled sample, it can be determined whether Co<sup>0</sup>/CoO or Co<sup>0</sup>/Co<sub>3</sub>O<sub>4</sub> are present as composite systems in core-shell structures or as individual phases. A shifted hysteresis loop under field-cooled conditions represents a core/shell structure [1]. An example of this is given in Fig. 4 for the 5% Co/xerogel sample. Here the hysteresis loop is shifted by 55 Oe when the sample is cooled in 10 kOe suggesting a core/shell structure for Co and CoO in this sample.

Another possibility for the cobalt state is that cobalt is incorporated substitutionally into the support (e.g as Co<sub>x</sub>Si<sub>1-x</sub>O<sub>2</sub>) or chemisorbed on the surface of the support with bonding provided by surface absorbed H<sub>2</sub>O and O<sub>2</sub>. In such cases, the  $\chi$  vs. T data follows the Curie-Weiss law:  $\chi = \chi_0 + [C/(T-\theta)]$  where C gives the concentration of the Co<sup>n+</sup> ions [4]. Furthermore, the variation of M vs. H at a low temperature (2 K) can be used to distinguish between Co<sup>2+</sup> and Co<sup>3+</sup> ions [4]. In the EMR studies of such materials, the presence of an EMR line at  $g = 4.3$  is definite confirmation of the presence of Co<sup>2+</sup> ions [6].

Next, the relationship between the different electronic states of cobalt and their concentrations with the F-T products and their distributions is discussed briefly.

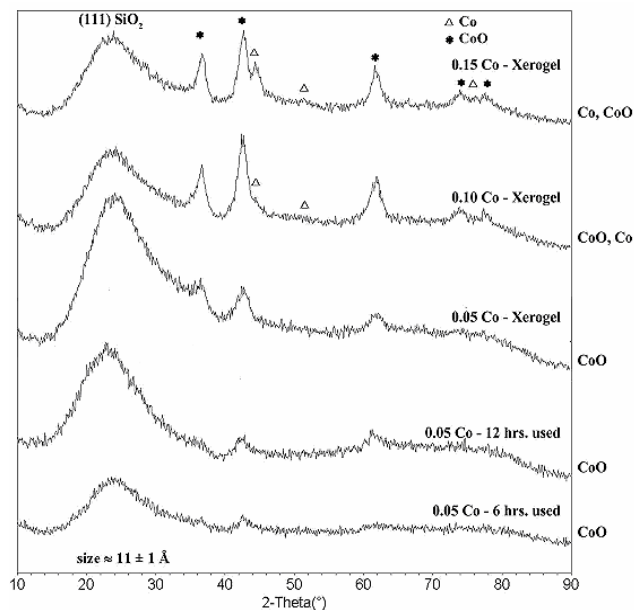


**Figure 1.** Room Temperature x-ray diffractograms of five samples of Co/xerogel with the peaks for Co<sup>0</sup>, CoO and SiO<sub>2</sub> identified. The size  $\approx 11$  Å is for SiO<sub>2</sub> [Ref. 1].

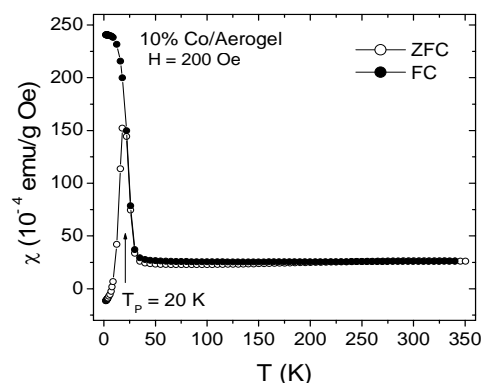


**Figure 2.** Temperature dependence of the magnetic susceptibility  $\chi$  of 10% Co/aerogel catalyst for the ZFC (zero-field cooled) and FC (field-cooled) cases.

In the conventional gas-phase FT synthesis at 240°C and 20 bar pressure, it was found that the presence of  $\text{Co}_3\text{O}_4$  yields higher methane selectivity whereas the presence of  $\text{Co}^{2+}$  species yielded lower methane selectivity but higher olefin selectivity [4]. Similarly why the FT activity of 10 % Co/aerogel catalysts is not much better than that of 6 % Co/aerogel [2] has been explained in our recent work [3] in that the 10% Co/aerogel contains unreduced CoO and a complex cobalt silicate in addition to the desired  $\text{Co}^0$ .

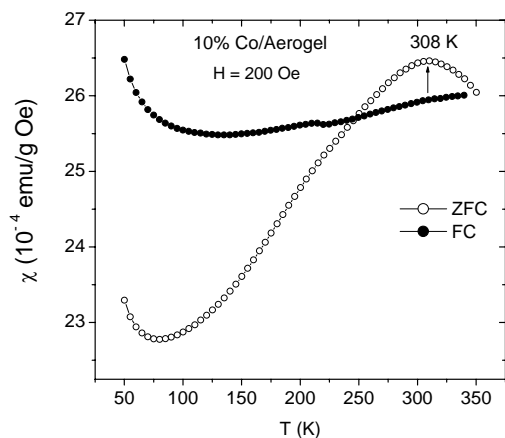


**Figure 3.** Expanded version of the  $\chi$  data of Figure 2 for higher temperatures.

### Conclusions

Here we have described how different electronic states and phases of cobalt in cobalt-based FT catalyst are determined using XRD, magnetometry and EMR spectroscopy. Such information is essential in understanding the nature of products and their distributions in FT synthesis.

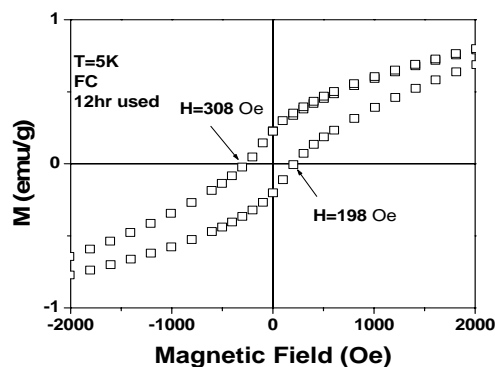
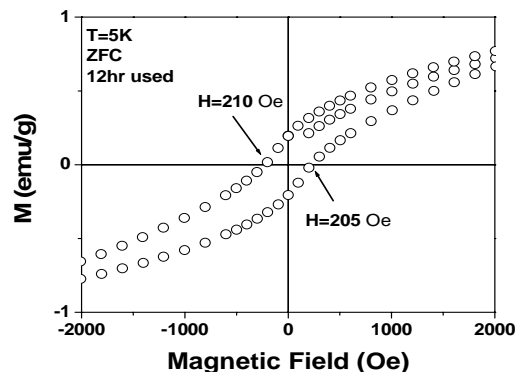


**Figure 4.** Hysteresis loops measured at 5 K for the 12-hr sample of 0.05 Co/aerogel under the ZFC and FC ( $H = 10$  kOe) conditions. The loop shift for the FC case supports the core/shell model discussed in the text.

### Acknowledgments

Support for this work was provided by the U. S. Department of Energy (Contract # DE-FC26-02NT41594). The authors thank Prof. Roberts (Auburn University) and Prof. Eyring (University of Utah), and their research groups for providing the samples used in this work.

### References

1. Dunn, B. C.; Convington, D. J.; Cole, P.; Pugmire, R. J.; Meuzelaar, H. L. C.; Ernst, R. D.; Heider, E. C.; Eyring, E. M.; Shah, N.; Huffman, G. P.; Seehra, M. S.; Manivannan, A.; Dutta, P.; *Energy Fuels*, **2004**, 18, 1519-1521.
2. Dunn, B. C.; Cole, P.; Convington, D. J.; Webster, M. C.; Pugmire, R. J.; Ernst, R. D.; Eyring, E. M.; Shah, N.; Huffman, G. P.; *Appl. Catal. A: General*, **2005**, 278, 233-238.
3. Dutta, P.; Dunn, B. C.; Shah, N.; Eyring, E. M.; Huffman, G. P.; Manivannan, A.; and Seehra, M. S.; (to be submitted).
4. Dutta, P.; Elbashir, N. O.; Manivannan, A.; Seehra, M. S.; and Roberts, C. B.; *Catalysis Letters*, **2004**, 98, 203-210.
5. Elbashir, N. O.; Dutta, P.; Manivannan, A.; Seehra, M. S.; and Roberts, C. B.; *Appl. Catal. A: General* **2005**, (In Press).
6. Manivannan, A.; Glaspell, G.; Dutta, P.; Seehra, M. S.; *J. Appl. Phys.* **2005**, (In Press).

# WHAT C-13 CHEMICAL SHIFT TENSORS CAN TELL US ABOUT METAL LIGAND INTERACTIONS IN CATALYSTS

Ronald J. Pugmire and Zhiru Ma

Department of Chemistry and Department of Chemical Engineering  
University of Utah

Catalysts will play an increasingly important role in the development of C1 chemistry and the production of hydrogen. The NMR group at Utah is now focusing on understanding subtleties in catalyst structure and function. We have recently focused our research on catalyst systems with the goal to explore the feasibility of obtaining FIREMAT data on various metal-ligand complexes. The FIREMAT<sup>1</sup> experiment has proven to be a very useful tool for obtaining carbon-13 chemical shift tensor data.

Twenty years ago low temperature shift tensor principal values were obtained in the Utah laboratory on a series of metal diene complexes<sup>2</sup> and some of these data were later included in an extended data set by Oldfield, et. al.<sup>3</sup> The earlier Utah data was obtained by fitting the powder patterns of the complexes and the error in these STPV's can be as high as 5-10 ppm. We have now begun to revisit this topic employing the high resolution FIREMAT technique. The additional resolution obtainable by this experimental technique has led to the discovery of additional resonance lines in the spectra of several metal-ligand complexes that we have recently studied. An illustrative example is found in the spectrum of (bicyclo[2.2.1]hepta-2,5-diene)dichloropalladium (II) in which the diene-carbons are split into a doublet separated by 2 ppm. This spectral feature is due to a break in the crystal symmetry arising from slight differences (~0.02 angstrom) in the palladium-diene bond lengths. The PVST data of these carbons are readily obtained from the FIREMAT data and these values are given in Table 1. Similar NMR data have been obtained in (1,5 cyclooctadiene)dimethylplatinum (II). These data illustrate the high degree of sensitivity to local structural variations. The data we have obtained at this writing have laid the ground work of a wider range of complexes that will be studied. We will begin modeling these data by means of quantum mechanical techniques in the next few months. Exploration of the relativistic effects on the ligands will be included in our modeling efforts.

**Table 1. Shift Tensor Principal Values in (bicyclo[2.2.1]hepta-2,5-diene)dichloropalladium(II)**

Carbon	$\delta_{iso}$	$\delta_{11}$	$\delta_{22}$	$\delta_{33}$
Diene (CH)	94.1	191.2	87.1	4.0
Diene (CH)	92.1	188.9	85.5	2.0
CH	66.1	100.1	68.7	29.6
CH2	52.4	66.1	56.0	35.0

## References

1. A Sensitive High-Resolution Magic-Angle-Turning Experiment for Measuring Chemical-Shift-Tensor Principal Values. D.W. Alderman, G. McGeorge, J.Z. Hu, R.J. Pugmire and D.M. Grant, 1998, Mol. Phys., 95, 1113-1126.

2. Low Temperature Solution Studies of Copper(I) Complexes and Trans-Cycloalkenes and Solid State <sup>13</sup>C NMR Studies of Metal-Diene Complexes, Gregory Michael Wallraff, Ph.D. thesis, Department of Chemistry, University of Utah, 1985.
3. Solid-State NMR and Density Functional Investigation of Carbon-13 Shielding Tensors in Metal-Olefin Complexes, R. Havlin, M. McMahon, R. Scinivasan, H. Le, and E. Oldfield, J. Phys. Chem. A **1997**, 101, 8908-8913.

**Acknowledgement.** This work was supported by the Department of Energy, NETL, as part of the Consortium for Fossil Fuel Science.

# OXYGENATE SYNTHESSES USING METHANOL PLASMAS

Yu Wang and Chang-jun Liu\*

Key Laboratory of Green Chemical Technology, School of Chemical Engineering, Tianjin University, Tianjin, 300072 China

## Introduction

Methanol can be produced from many feedstocks including renewable resource. It is an excellent alternative feedstock for syntheses of oxygenates, like acetic acid, ethylene glycol (EGL), aldehydes and others. Recently, we have theoretically investigated the feasibility of synthesis of EGL directly from the coupling of methanol [1]. An experimental study of methanol plasma using corona discharge has confirmed the possibility of this reaction [2]. In this work, we attempt to compare methanol conversions using corona discharge and dielectric-barrier discharge (DBD).

## Experimental and Setup

Corona discharge reactor applied in this work has been previously reported [2]. The reactor is a quartz tube with an inner diameter of 6 mm. A cylindrical furnace is placed around the reactor for the reaction temperature control. This discharge reactor consists of two electrodes, a top metal wire electrode and a lower hollow electrode as the grounded one. The gap between the electrodes is fixed at 6 mm. The high voltage amplifier (Trek 20/20B), connected with a HP33120A signal generator, supplies a high voltage with DC or AC (at different waveforms) signal to the top wire electrode.

The DBD reactor used in this work was similar to that reported previously [3]. Discharge zone lies between a dielectric-barrier made of quartz and a stainless steel tube serving as grounded electrode with a length of 250 mm and a gap width of 1.1 mm. An aluminum foil is connected with a high voltage generator, which output a sinuous signal at a frequency of 25 kHz. Methane and carbon monoxide were introduced into the discharge gap (between the grounded electrode and quartz surface) both at 20 ml/min via two mass flow controllers.

The voltage and current were measured with a high voltage probe (Tektronix P6015 A) and a pulse current transformer (Pearson Electronics 411) via a digital oscilloscope (LeCroy Model LC 334A) (for AC). The discharge power was measured via a digital multimeter (Keithley 2000).

The feed gases and gaseous products were analyzed with an on-line gas chromatograph (HP 5890 with TCD and FID) and mass selective detector (HP 5971).

## Results and Discussions

The previous DFT study has identified the reaction routes of methanol dissociation based on the grounded state. Methanol is dissociated by routes: methanol dissociation to  $\text{CH}_3\text{O}\cdot + \cdot\text{H}$ ,  $\cdot\text{CH}_2\text{OH} + \cdot\text{H}$  and  $\cdot\text{CH}_3 + \cdot\text{OH}$ . The calculated energies for these three pathways using the B3P86 method are 100.56, 94.35 and 89.54 kcal/mol, respectively. The calculated results show that the dissociation of methanol to  $\cdot\text{CH}_3$  and  $\cdot\text{OH}$  requires less energy and is the dominating dissociation route. Just a little more energy requested for the formation of  $\cdot\text{CH}_2\text{OH}$ , compared to the formation of methyl radical. The dissociation of methanol into  $\cdot\text{CH}_3\text{O}$  and  $\cdot\text{H}$  is most difficult. Evidently,  $\cdot\text{CH}_3$ ,  $\cdot\text{CH}_2\text{OH}$  and  $\text{CH}_3\text{O}\cdot$  can be obtained from methanol dissociation. Theoretically, the recombination of these radicals will generate several products including ethane, ethylene glycol, ethanol and dimethyl ether (DME).

The experimental investigation confirms that, using corona discharge, EGL can be produced directly from methanol, as shown in Table 1. In addition to EGL, CO, ethanol, propanol and trace ethane

have also been produced. No DME was observed. With the present reactor design, the AC corona discharge leads to a more production of EGL. Compared to the negative corona discharge (DC-neg), the positive corona (DC-pos) is more favored for EGL synthesis. Also, the positive corona discharge generates more ethanol and propanol. At the present design of reactor system, however, the major product from methanol conversion using corona discharges (including AC and DC corona discharges) is syngas. The corona discharge is too energetic that the oxygenated hydrocarbon products will be destroyed quickly once they formed.

**Table 1. Production Rate of Methanol Dissociation Using Corona Discharges**

	Production rate ( $\mu\text{mol}/\text{min}$ )				
	CO	ethanol	propanol	EGL	ethane
DC-pos	169.1	0.007	0.06	0.8	trace
DC-neg	250.6	0.004	0.01	0.1	trace
AC-sin	328.0	1.9	3.6	8.7	trace

On the other hand, the experimental investigation using DBD plasmas exhibits a very different result (i.e., very different product distribution). Under the influence of DBD plasmas, the major product is still syngas. Some minor oxygenate products from this DBD plasma methanol conversion include aldehydes, acids (principally,  $\text{HCOOH}$ ), and alcohols (with EGL). The oxygenate with highest selectivity (5.5%) is formic acid. The selectivity of EGL is 1.2%.

For either corona discharge or DBD, in order to increase the yields of oxygenates, it is important to keep the oxygenate molecules stable within the energetic discharges once they are formed. We have observed that the liquid drops within the discharges can help to remain the oxygenate molecules. It is potential to develop a liquid plasma technology for the oxygenate syntheses directly from methanol.

## Summary

The present investigation has confirmed that different discharge plasmas will induce a different product distribution. The corona discharge can convert methanol directly into EGL and alcohols, while DBD can induce a synthesis of aldehydes and acids. The theoretical study has confirmed the feasibility of this kind of synthesis, which has major advantage with simple operation and small setup required. The drawback of the present synthesis is the low yield of objective oxygenates products. For future development, a liquid plasma conversion technology will be developed.

**Acknowledgement.** Part of equipment and setup were donated by ABB Switzerland Ltd. Support from Major Research Project of National Natural Science Foundation of China (No. 20490200) is very appreciated.

## References

- (1) Cheng, D.-G.; Wang, J.-G.; and Liu, C.-J. *DFT Study of Methanol Dissociation*, paper submitted.
- (2) Li, H.-Q.; Zou, J.-J.; Zhang, Y.-P.; and Liu, C.-J. *Chem. Lett.* **2004**, 33, 744-745.
- (3) Wang, Y.; Liu, C.-J.; Zhang, Y.-P. Plasma methane conversion in the presence of dimethyl ether using dielectric-barrier discharge, *Energy Fuels* (accepted).

# A THERMOSTABLE CU-MN BASED CATALYST FOR HIGH TEMPERATURE WATER-GAS-SHIFT REACTION

Quangsheng Liu, Runxia He, Xieli Cu, Keduan Zhi, Wenping Ma\*

Department of Chemical Engineering, Inner Mongolia University of Technology, Hohhot, P. R. China, 010062

## Introduction

The water gas shift reaction (WGSR),  $\text{CO} + \text{H}_2\text{O} \rightarrow \text{CO}_2 + \text{H}_2$ , is an industrially important route to  $\text{H}_2$  production and plays an important role in many current technologies such as methanol synthesis, methanol steam reforming, ammonia synthesis, coal gasification, as well as fuel cell technology<sup>[1]</sup>.

Even though the chromium-promoted iron-based shift catalyst have shown excellent activity, high stability and certain resistance to the sulfur poisoning at 315-450°C, the existence of chromium in this catalyst make it environmental restrictions and press for discarding of chromium compounds. In addition, in order to avoid the  $\text{Fe}_3\text{O}_4$  being reduced to metallic iron, which will catalyze the F-T synthesis reaction, large superfluous amount of steam must be used, which lead to the increasing of the operation costs. So radical solution to avoid the by-product formation is to replace the classical iron-base high temperature shift catalyst by an iron free catalyst capable of operation at these conditions<sup>[2]</sup>. Most of investigation about the iron free high temperature shift catalyst are the Cu-based high temperature shift catalyst<sup>[3-7]</sup>. All of these Cu-based high temperature shift catalyst can used in lower steam/gas ratio and show excellent resistance to the F-T side reaction less than 400 °C. However, the reaction temperature high than 450°C result in the activity of the catalyst decrease badly. Moreover, even the reaction temperature restore less than 400 °C the activity cannot restore. This means the mentioned Cu-based high temperature shift catalyst have bad resistance to high-temperature excursion higher than 400°C. This shortcoming restricts the popularization of the Cu-based high temperature shift catalyst. The present paper reports the results of a new Cu-Mn-Based catalyst for water gas shift catalyst that can be comparable to current used iron-based catalyst.

## Experimental

**Catalyst Synthesis.** All reagent used were of an analytical grade. The Cu-Mn catalysts samples were prepared using the co-precipitation technique. Details of preparation procedures and characteristic were reported elsewhere<sup>[8]</sup>. In brief, the Cu-Mn based catalysts were precipitated with copper sulfite and manganese sulfite by alkali solutions in a beaker. The resulting slurry was subsequently aged followed by washing, drying and calcinations.

**Fixed-Bed Reactor Test.** The activity of Cu-Mn based (12-14 mesh, 0.5g) was examined in a bench-scale fixed-bed stainless steel reactor (ID = 6mm) under atmospheric pressure, 350 °C and 3000 h<sup>-1</sup> (dry-gas basis). The composition of feed gas was 12% CO, 18% CO<sub>2</sub>, 56% H<sub>2</sub> and 16% N<sub>2</sub> (internal standard). Prior to WGS reaction, the catalyst samples were reduced using the same reactant gas mixture

under severe conditions: 530 °C, 3000 h<sup>-1</sup> for 15 h. The gas compositions before and after the WGS reaction were analyzed online by a GC-8A gas chromatograph (GC).

**Characterization Methods.** The BET surface areas of the catalysts were measured by isothermal adsorption of N<sub>2</sub> at 77K using a surface area porosity analyzer ASAP2010. X-Ray powder diffraction (XRD) analysis of the samples were performed on D8 Advance X-ray diffraction-meter, Cu K $\alpha$  radiation with a nickel filter was used with a power of 40 kV  $\times$  40 mA. The samples morphology(TEM) was studied on a JEM-2010 electron microscope. Thermal-Analysis were performed with DTG-50/50H.

## Results and Discussion

Table 1 lists the bulk composition, BET surface areas before and after WGS reaction and CO conversion ( $X_{\text{CO}}$ , %) at 350 °C of the catalysts samples. The same experimental data of a commercial Fe-Cr WGS catalyst denoted as C12-4, which was supplied by United Catalyst Inc. (UCI), are also listed in Table 1 for comparison. The BET surface areas of both catalysts before reaction are 52.4 and 70.2m<sup>2</sup>/g, respectively. Both BET surface areas of Cu-Mn catalyst before and after reaction are lower than that of C12-4 catalyst correspondingly. After WGS reaction, the BET surface areas of Cu-Mn and C12-4 catalysts were decreased to 30.4 m<sup>2</sup>/g and 40.4 m<sup>2</sup>/g, respectively. But the decrease scope of Cu-Mn(42%) is almost same as that of C12-4. CO conversions at 350 °C during steady state for both catalysts are high and the activity of Cu-Mn is 11% higher than that of C12-4, which was not quantitatively correlated well with their surface areas. Due to the Cu-Mn and C12-4 catalysts experiencing very severe thermo-resistance test during reduction period (530 °C and 15 hours), the high CO conversions showed that both catalysts had excellent thermo-resistance property.

Table 1. Summary of BET and Reaction Results of Cu-Mn and C12-4 catalysts

Catalyst ID	CO Conversion % <sup>a</sup>	Special surfacearea m <sup>2</sup> /g	
		Before reaction	After reaction
Cu-Mn	64.7	52.4	30.4
C12-4	53.8	70.2	40.4

<sup>a</sup>  $X_{\text{CO}}$ , % = (CO mole flow rate in - CO mole flow rate out)/ CO mole flow rate in  $\times$  100

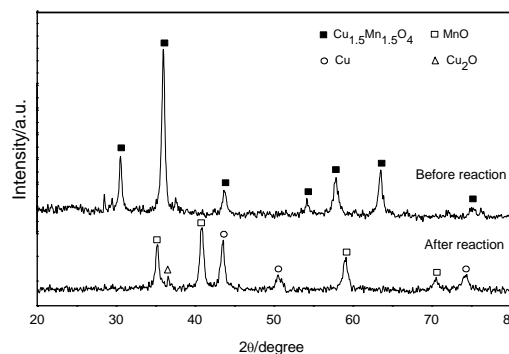


Fig.1 X-ray powder diffraction patterns of Cu-Mn catalyst before and after reaction

XRD spectra of the Cu-Mn catalysts before and after reaction are shown in Fig.1. The main crystal phase of this type Cu-Mn catalyst before reaction is single spinel structure-Cu<sub>1.5</sub>Mn<sub>1.5</sub>O<sub>4</sub> with small amount of unidentified phase ( $2\theta=25-30^\circ$ ). No obvious other

\* Present address: Department of Chemical Engineering, West Virginia University, Morgantown, WV. 26505

crystallization is found. The crystal phase of this type Cu-Mn catalyst after reaction is mixture of three crystallization- MnO, Cu and Cu<sub>2</sub>O, of which the Cu micro-crystallization is more than 90% of Copper component.

The thermo-analysis (TGA and DTA) is shown in Fig.2. A weight loss with an endothermic peak near 46°C is attributed to dehydration of adsorbed water. It is followed by a gradual weight loss till 292°C with an obvious exothermic peak, which can be assigned to forming of Cu<sub>1.5</sub>Mn<sub>1.5</sub>O<sub>4</sub> from its precursor. A metastable endothermic peak appears near 482°C, which can be attributed to the forming of an new undetermined crystallization phase corresponding to 2θ=25-30° in XRD spectra.

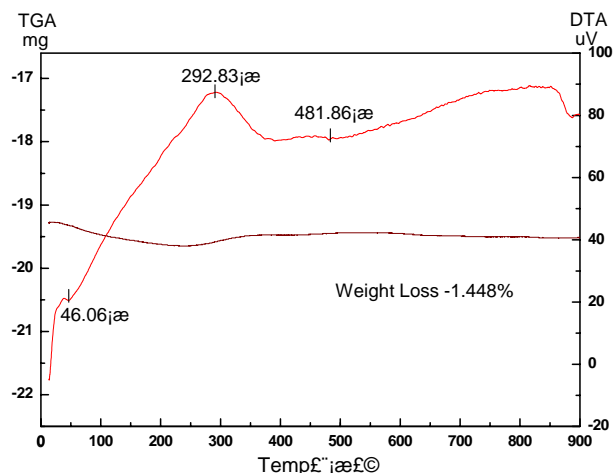


Fig.2 DTA/TGA trace of Cu-Mn catalyst after dryness

Transmission electron micrographs of Cu-Mn catalysts before

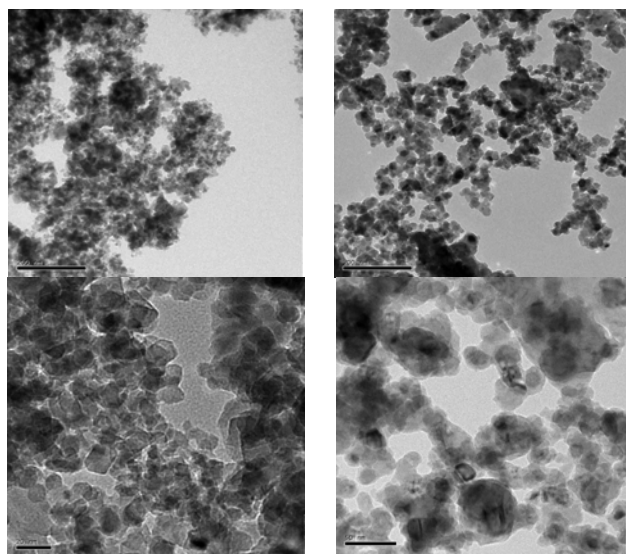


Figure 3. Transmission electron micrographs of Cu-Mn Catalyst

Left: Before reaction; Right: After reaction

and after reaction are shown in Fig. 3. The Cu-Mn catalysts before and after reaction are composed of clubbed, flake and polyhedron particle. The particle sizes before reaction distribute from 10nm to

50nm. After reaction the particles sizes increase and distribute narrower than that before reaction. There appears micro-crystal on the flake particle after reaction, which is speculated to the Cu crystal resulted from reducing of Cu<sub>1.5</sub>Mn<sub>1.5</sub>O<sub>4</sub>.

### Concluding Remarks

It can be concluded that the Cu-Mn based catalyst gives appreciably higher activity when compared to existed industrial high temperature shift catalysts based on iron/chromium oxides and additionally this catalyst system is a potentially superior catalysts in comparison to the current industrially operated iron/chromium oxides high temperature shift catalysts. It is a good alternative to the traditional high-temperature Fe-Cr WGS catalysts.

**Acknowledgement.** This study was supported by Natural Science Foundation of China (20066002) and Science Foundation of Inner Mongolia (20041001) in China.

### References

- (1) N. Schumacher, A. Boisen, S. Dahl, J. Catal., 2005, 229: 265-275
- (2) Jack H. Carstensen, John B. Hansen, Peter S. Pederson, New Developments in High Temperature Shift Catalyst Technology Solve the Fishcher-Tropsch Problem, 1989 AICHE Ammonia Safety Symposium, San Francisco
- (3) N. Yamamoto, B. Hashimoto, H. Shibano, Kokai Tokkyo Koho JP, 63/77546, 988.
- (4) F. M. Gottschalk, G. J. Hutchings, Appl. Catal., 1989, 51: 127-139.
- (5) Sh. B. Feng, R. Liang, X. D. Dong, Chinese J. Catal., 1996, 17: 391-393.
- (6) Y. Tanaka, T. Utaka, R. Kikuchi, Appl. Catal., A: General, 2003, 242: 287-295.
- (7) Y. Tanaka, T. Utaka, R. Kikuchi, J. Catal., 2003, 215: 271-278.
- (8) Yunxia He, Preparation and Characteristics of Fe-Based, Cu-Based and RE-Based Water Shift Catalysts for Production of Hydrogen in Fuel Cell, Master Degree Dissertation, Inner Mongolia University of Technology, 2004.